REPORT DOCUMENTATION PAGE

Public reporting burden for this collection of information is estimated to average 1 hour per response, including the time for reviewing maintaining the data needed, and completing and reviewing this collection of information. Send comments regarding this burden es suggestions for reducing this burden to Department of Defense, Washington Headquarters Services, Directorate for Information Ope Suite 1204, Arlington, VA 22202-4302. Respondents should be aware that notwithstanding any other provision of law, no person sh ...., ...g to comply with a collection of information if it does not display a currently valid OMB control number. **PLEASE DO NOT RETURN YOUR FORM TO THE ABOVE ADDRESS.**

1. REPORT DATE (DD-MM-YYYY)	2. REPORT TYPE	3. DATES COVERED (From - To)
22-12-2008	Annual Technical Report	01-04-2007 to 14-09-2008

4. TITLE AND SUBTITLE	5a. CONTRACT NUMBER
Micro-Structured Materials for Generation of Coherent Light And Optical Signal Processing	5b. GRANT NUMBER FA9550-05-1-0180
	5c. PROGRAM ELEMENT NUMBER

6. AUTHOR(S)	5d. PROJECT NUMBER
M.M. Fejer, R.K. Route, M. Charbonneau-Lefort, J. Huang, D. Hum, P. Kuo, C. Langrock,	5e. TASK NUMBER
	5f. WORK UNIT NUMBER

7. PERFORMING ORGANIZATION NAME(S) AND ADDRESS(ES)	8. PERFORMING ORGANIZATION REPORT NUMBER
Edward L. Ginzton Laboratory Stanford University Stanford, CA 94305-4088	SPO No. 33301

9. SPONSORING / MONITORING AGENCY NAME(S) AND ADDRESS(ES)	10. SPONSOR/MONITOR'S ACRONYM(S)
AFOSR 801 North Randolph Street, Room 732 Arlington, VA 22203-1977	
	11. SPONSOR/MONITOR'S REPORT NUMBER(S)

12. DISTRIBUTION / AVAILABILITY STATEMENT
Approved for public release; distribution unlimited.

13. SUPPLEMENTARY NOTES
The view, opinions and/or findings contained herein are those of the author(s) and should not be construed as necessarily representing the official policies or endorsements, either expressed or implied, of the Air Force Office of Scientific Research or the U.S. Government.

14. ABSTRACT

Our research interests focus on improving nonlinear optical materials, developing microstructuring techniques to access new wavelength regions and new applications, and fabricating devices for high-power visible generation, ultra-fast optical interactions, mid-IR generation, and optical signal processing.

This program has continued the development of microstructured nonlinear optical materials and quasi-phase-matched devices based on those materials. The material systems investigated, periodically-poled ferroelectrics, especially lithium niobate (PPLN) and lithium tantalate (PPLT), and orientation-patterned GaAs (OP-GaAs), enable nonlinear interactions impossible in conventional nonlinear media. This work included characterization of vapor-transport-equilibrated near-stoichiometric ferroelectrics, enhancements in periodic-poling technology, and development of improved proton-exchanged waveguide techniques. Following the materials characterization and improved processing techniques, we have been able to fabricate new devices including OP-GaAs devices for broadband optical parametric generation (OPG) at mid-infrared wavelengths, wide bandwidth parametric amplifiers in aperiodic QPM structures, high power visible light generation including the sodium yellow line, and reverse-proton-exchanged PPLN waveguide devices for quasi-group-velocity-matching, optical signal processing, and generation of nearly-transform-limited OPG.

15. SUBJECT TERMS
microstructured nonlinear optical materials, quasi-phasematched devices, periodically-poled lithium niobate, orientation-patterned GaAs, stoichiometric lithium tantalate, frequency conversion, non-linear optics

16. SECURITY CLASSIFICATION OF:			17. LIMITATION OF ABSTRACT	18. NUMBER OF PAGES	19a. NAME OF RESPONSIBLE PERSON Martin M. Fejer
a. REPORT	b. ABSTRACT	c. THIS PAGE		40	19b. TELEPHONE NUMBER (include area code) (650) 725-2160

Standard Form 298 (Rev. 8-98)
Prescribed by ANSI Std. Z39.18

Annual Technical Report, Cont.

1. AFOSR GRANT NUMBER: FA9550-05-1-0180

2. PERIOD COVERED BY REPORT: 04/01/2007 – 09/14/2008

3. TITLE OF PROPOSAL: Micro-Structured Materials for Generation of Coherent Light
                            And Optical Signal Processing

4. LIST OF MANUSCRIPTS SUBMITTED OR PUBLISHED UNDER AFOSR
    SPONSORSHIP DURING THIS REPORTING PERIOD
    a) Mathieu Charbonneau-Lefort, Bedros Afeyan and M. M. Fejer,"Optical parametric amplifiers
        using chirped quasi-phase-matching gratings. II. Space-time evolution of light pulses", J. Opt. Soc.
        Am. B, Vol. 25, pp.683-700 (April 2008)
    b) Mathieu Charbonneau-Lefort, Bedros Afeyan and M. M. Fejer,"Optical parametric amplifiers
        using chirped quasi-phase-matching gratings I: practical design formulas", J. Opt. Soc. Am. B,
        Vol. 25, pp.463 (March 2008)
    c) P. S. Kuo, K. L. Vodopyanov, M. M. Fejer, X. Yu, J. S. Harris, D. F. Bliss, and D. Weyburne,,
        "GaAs optical parametric oscillator with circularly polarized and depolarized pump", *Optics
        Letters*, No. 18, Vol. 32, pp.2735-2737 (September 2007)
    d) Carsten Langrock and M. M. Fejer,"Background-free collinear autocorrelation and frequency-
        resolved optical gating using mode multiplexing and demultiplexing in reverse-proton-exchange
        aperiodically poled lithium niobate waveguides", *Optics Letters*, No. 16, Vol. 32, pp.2306-2308
        (August 2007)
    e) Jie Huang, Carsten Langrock, X. P. Xie, and M. M. Fejer,"Monolithic 160 Gbit/s optical time-
        division multiplexer", *Optics Letters*, No. 16, Vol. 32, pp.2420-2422 (August 2007)
    f) Carsten Langrock and Martin M. Fejer,"Fiber-feedback continuous-wave and synchronously-
        pumped singly-resonant ring optical parametric oscillators using reverse-proton-exchanged
        periodically-poled lithium niobate waveguides", *Optics Letters*, No. 15, Vol. 32, pp.2263-2265
        (July 2007))
    g) D. S. Hum, R. K. Route, G. D. Miller, V. Kondilenko, A. Alexandrovski, J. Huang, K. Urbanek,
        R. L. Byer, and M. M. Fejer,"Optical properties and ferroelectric engineering of vapor-transport-
        equilibrated, near-stoichiometric lithium tantalate for frequency conversion", Journal of Applied
        Physics, No. 9, Vol. 101, pp.093108 (May 2007)
    h) D. S. Hum, R. K. Route and M. M. Fejer,"Quasi-phase-matched second-harmonic generation of
        532 nm radiation in 25-degree-rotated, x-cut, near-stoichiometric, lithium tantalate fabricated by
        vapor transport equilibration", Optics Letters, No. 8, Vol. 32, pp.961-3 (April 2007)
    i) Xiuping Xie and M. M. Fejer,"Cascaded optical parametric generation in reverse-proton-exchange
        lithium niobate waveguides", JOSA B, No. 3, Vol. 24, pp.585-591 (March 2007)

5. SCIENTIFIC PERSONNEL SUPPORTED BY THIS PROJECT AND DEGREES
    AWARDED DURING THIS REPORTING PERIOD:

            Faculty - M.M. Fejer
            Senior Staff - R. Route, K. Vodopyanov
            Staff – C. Langrock
            Post-Doctoral Associate – P.S. Kuo, O. Levi
            Students – D. Chang, M. Charbonneau-Lefort (Ph.D. awarded 2007), J. Huang (Ph.D.
                    awarded 2007) , D. Hum (Ph.D. awarded 2007), P. Kuo (Ph.D. awarded
                    2008), C. Langrock (Ph.D. awarded 2007), A. Lin

20090113295

6. REPORT OF INVENTIONS BY TITLE ONLY

7. SCIENTIFIC PROGRESS AND ACCOMPLISHMENTS: See Final Technical Report

8. TECHNOLOGY TRANSFER:
   This program explores micro-structured nonlinear optical materials and quasi-phasematched (QPM) nonlinear devices based on them. Technology developed under this and predecessor programs has let to numerous collaborations with industry and academic institutions. Most recently we have collaborated with LLNL, MIT Lincoln Labs, CeLight, Sony, UCSC (Center for Adaptive Optics), Purdue, USC, U. New Mexico.

9. CORRESPONDENCE ADDRESS:
   Martin M. Fejer, P.I.
   Ginzton Laboratory, Mail Code 4088   (tel) 650-725-2160
   Stanford University   (fax) 650-723-2666
   Stanford, CA 94305-4088   fejer@stanford.edu

Table of Contents

I. Introduction

This annual technical report summarizes progress during the final reporting period of a 42-month program with AFOSR support under FA9550-05-1-0180 (03/15/05 - 09/14/08) on micro-structured materials for generation of coherent light and optical signal processing. This program is a continuation of research carried out under AFOSR awards, F49620-99-1-0270 and F49620-02-1-0240.

II. Technical Report

II.1 Materials

II.1.1 Ferroelectric Materials

Stoichiometric Lithium Tantalate (D. Hum)

Our work to date has established that the vapor-transport equilibration (VTE) method is capable of producing crystals of both lithium niobate (LN) and lithium tantalate (LT) that are closer to stoichiometry than those produced by growth from congruent melts or from lithium-rich melts. In stoichiometric lithium tantalate (SLT), the reduction in anti-site tantalum point defects (by approximately two orders of magnitude) has two key effects: the photoconductivity is increased in proportion to the reduction in defect density (presumably through an increase in the carrier lifetime) and the coercive field for domain reversal is also reduced by approximately two orders of magnitude (as low as 60 V/mm compared to 20 kV/mm in congruent crystals). The increase in photoconductivity without a concomitant increase in photogalvanic current results in the elimination of measurable room-temperature photorefractive damage, and easier poling of thicker wafers. We have continued to measure important characteristics such as absorption and optical damage threshold in VTE SLT as they pertain to the application of this material in frequency conversion applications.

a. Absorption in Stoichiometric Lithium Tantalate

In the absence of photorefraction, thermal loading due to optical absorption in nonlinear materials ultimately limits the average-power handling capabilities. To measure the absorption of stoichiometric lithium tantalate fabricated by vapor-transport equilibration (VLT), several measurement tools and experimental techniques were employed. In the ultraviolet, a Cary 500 Spectrophotometer was used to measure the ordinary-wave transmission of both congruent lithium tantalate (CLT) and VLT. The absorption was then calculated from the transmission spectra. To measure the extraordinary wave a SOPRA spectroscopic ellipsometer aligned in transmission mode was used. Ordinary wave measurements were also measured via the spectroscopic

ellipsometer and were in good agreement with Cary 500 spectrophotometric data. Absorption of both VLT and CLT are shown in fig. 1 (left).
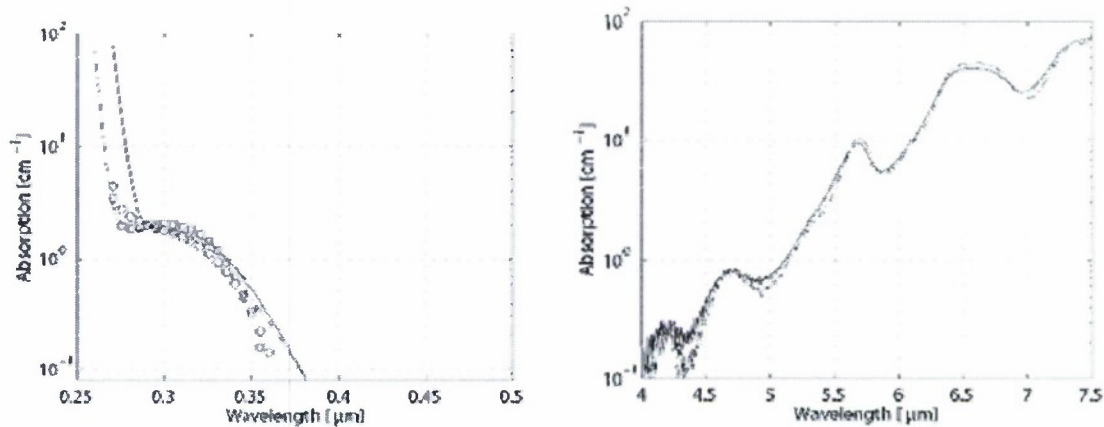

Figure 1: (left) Ordinary and extraordinary absorptions for both CLT and VLT. CLT ordinary-wave absorption measured on the Cary 500 Spectrophotometer is shown as the solid curve. VLT ordinary-wave absorption measured on the Cary 500 Spectrophotometer is shown as the dashed curve. Circles and squares represent extraordinary-wave and ordinary-wave VLT absorption measured on the ellipsometer. (right) Ordinary wave absorptions for both congruent LT (solid) and VLT (dashed) in the mid-infrared.

To measure the mid-infrared absorption, a BioRad FTS-40 FTIR spectroscope was used. CLT. Figure 1 (right) shows both CLT and SLT absorption. VLT samples show somewhat narrowed multi-phonon absorption resonances.

b. Laser-induced-damage threshold in Stoichiometric Lithium Tantalate

For high energy pulses, surface or bulk optical damage will often limit the peak power capabilities of nonlinear crystals before absorption becomes the limiting factor. To measure this effect, 3-mm-long, uncoated samples of congruent lithium niobate, CLT and VLT were polished and cleaned. A 12-ns-pulsewidth, Q-switched, 2.4-mJ, 10-Hz-repetition-rate, 1064-nm Nd:YAG laser was loosely focused to a 55 μm spot (1/e2-intensity radius) into the crystal. Damage statistics are plotted in fig. 2 with the number of test spots (N) for each sample indicated. Measured energy damage thresholds for congruent lithium niobate, CLT and VLT are 2.3 J/cm2, 7.3 J/cm2 and 7.3 J/cm2 respectively for a 55 μm radius optical beam. For all congruent lithium niobate samples tested, surface damage was the dominant damage mechanism. For both CLT and VLT, however, all samples damaged in the bulk before the surface. The statistics suggest that the damaging defects in LT are incorporated during the melt growth of the original CLT substrates, rather than during the VTE process.

Stoichiometric MgO:Lithium Niobate (R. Roussev)

Periodically-poled lithium niobate remains of significant interest because its nonlinear optical coefficient is higher than that of lithium tantalate. So far, no demonstration has been made of non-doped near- lithium that is free of optical damage, either near-stoichiometric or congruent composition. Our efforts focused mainly on developing damage-resistant VTE crystals with light MgO-doping (0.3-1.0 mol %).

The space-charge field is a convenient measure of the photorefractive sensitivity of the crystal. Due to the large electro-optic coefficient R_{33}, the saturated space-charge field in lithium niobate must be less than 10 V/mm to enable frequency-conversion applications without significant wavefront distortion. A plot of the

saturated space-charge field versus crystal weight-gain during VTE, shown in fig. 3, demonstrates how vapor phase equilibration of 1 mol-% MgO-doped lithium niobate reduces its photorefractive sensitivity. (We typically measure the saturated space-charge field as that generated by high-intensity green light (0.7 W at 514 nm, in a ~70-80 μm beam diameter)).
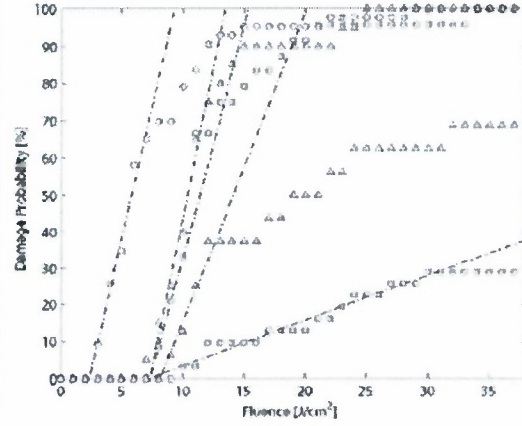

Figure 2: Damage probabilities for congruent lithium niobate (circles, N=43) and two samples of both CLT (triangles, N=20,16) and VLT (squares, N=31,24).

VTE experiments with 0.51-mm-thick 0.3-mol% MgO-doped LN showed that very low saturated space-charge fields of 0.5-1.0 V/mm can be achieved with ~350-hour equilibration in Li-rich powder at 1100 °C. Such low space-charge fields, more than three orders of magnitude lower than that in optical-grade commercial congruent lithium niobate, poses no problem for any device applications in nonlinear optics. The space-charge field is also three to five times lower than that in the best 5% MgO-doped commercial crystals. Because we measure the space-charge field by propagating the intense green laser beam along the crystal c-axis, the polarization of the light is ordinary. Most applications utilize light with extraordinary polarization to make use of the largest component of the nonlinear or electro-optic tensor. A crystal with low space-charge field was subjected to a high-intensity laser beam at 514 nm propagating along its a-axis and extraordinarily
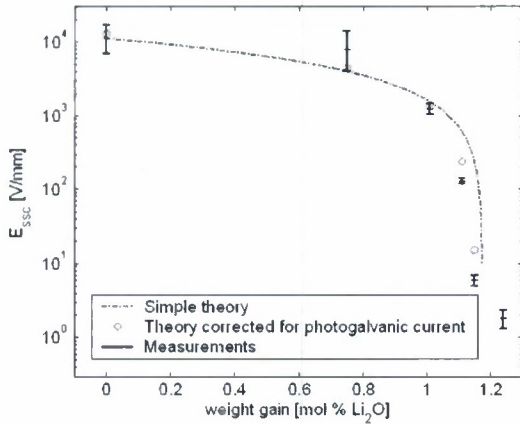

Figure 3: Saturated space-charge field as a function of molar weight gain during VTE of 1 mol% MgO-doped lithium niobate.

polarized, as is used for conventional QPM SHG. No signs of beam fanning were observed at the maximum available power of 600 mW with a beam diameter of ~70-80 μm. In comparison, in congruent LN, drastic beam fanning happened in less than 3 seconds at 90 mW. This experiment proved that our way of measuring the space-charge field provides an adequate tool for characterizing the photorefractive properties of the

3

crystal for practical purposes. The lightly-MgO:doped crystals appear lightly yellow-to-red-in color after the VTE process when viewed from the side through the edges of the wafers. This raised a concern that there may be increased absorption in the blue and green region compared to the original crystals, which could limit the power-handling capabilities of the crystal.

Transmission spectra with low-intensity light propagating along the c-axis in the plane of a VTE-processed wafer showed very slightly increased absorption in the 370-500 nm waveband as compared to the original congruent composition crystal. High-intensity measurements were performed using the photo-thermal common-path interferometry (PCI) technique. The results showed that the absorption of the VTE crystal under high-intensity illumination is no greater than the absorption of commercial 5% MgO:doped LN. It appears that the slight coloration of the crystal is due to a small number of color centers and is quickly bleached under high intensity illumination. Therefore, it does not pose a problem for visible-light generation. The results of the above experiments were first described in a conference presentation and contributed paper at Photonics West 2006 [Roussev 1].

In order for VTE-SLN to be practical, a full-wafer fabrication process is necessary. The main problems that arose with VTE on large samples and whole wafers were wafer bowing and twinning. We developed a process where wafer twinning can be avoided and where wafer bowing is minimized. In the last four wafers processed, bowing was less than 100 μm from center to edge which was easily dealt with in the subsequent fine-grinding and re-polishing steps. In addition, the three of the four were virtually free of twinning.

Some significant advances in the domain patterning of lightly MgO-doped VTE-SLN described in the following section on periodic poling, allowed the fabrication of a bulk chip for high-power CW second harmonic generation of green coherent radiation. The 330-μm thick 0.3-% MgO:SLN wafer was periodically-poled with a period of 7.1 μm over a 1.5 cm length. With near-optimum focusing, 1.3 W of 532 nm green light was generated for several hours near room temperature without any signs of degradation. The green output power was limited by the conversion efficiency of the grating and the available pump power (10 W at 1.064 μm). Better quality periodic poling should lead to a 2.5- fold increase in normalized efficiency. We can expect to obtain periodic poling of very good quality on 0.27-0.3 mm thick crystals that have apertures adequate for SHG under focusing conditions optimized in crystal lengths of 2-3 cm. These improvements will allow testing of the power-handling limits of this material. The results on high-power CW green SHG were also first presented at Photonics West 2006.

II.1.2 Periodic Poling Technology

Periodic poling of VTE- MgO:SLN (R. Roussev)
At the Photonics West 2006 conference, early results on periodic poling of SLN of various doping levels were presented [Roussev 1]. It was determined that lower doping levels allowed for better regularity of the periodic structures and shorter periods (fig. 4). Periodic poling of good quality with periods as short as 10 μm was obtained in 0.4-mm thick 0.3-% MgO:SLN. The quality of poling started to degrade for periods shorter than

Figure 4: Periodic poling of LN with different doping levels: (Left to righ)t: 5-% MgO:CLN, period=15 microns; 1-% MgO:SLN, period=15 microns; Non-doped SLN, period=8 microns; 0.3-% MgO:SLN, period=10 microns; 0.3-% MgO:SLN, period=8 microns.

8 μm. The method of periodic poling utilized a simple single-lithography process where trenches in hard-baked photoresist were used as contacts for liquid electrolyte electrodes for periodic poling. The simple preparation of the electrodes and room-temperature poling would allow lower-cost devices. Measurements of the dependence of domain-wall velocity (fig. 5) and nucleation density on the applied electric field allowed for a better understanding of the material properties for periodic poling and further optimization of the electrode preparation and poling voltage waveform in order to improve poling quality and achieve shorter poling periods. As a result, periodic poling of very good quality was achieved in 0.3 and 0.5-% MgO:SLN for periods of 9.6 and 16 μm, appropriate for yellow-light generation and waveguide devices for optical-signal processing at 1.55/0.775 μm, respectively. In addition, gratings of periodic poling of acceptable quality were obtained on a 0.33-mm thick 0.3-% substrate with a length of 1.5 cm (fig. 6). Although periodic poling of 0.3-% MgO:SLN is slightly easier than of 0.5% MgO:SLN, the difference is small enough to permit choosing a wafer composition based on other properties.
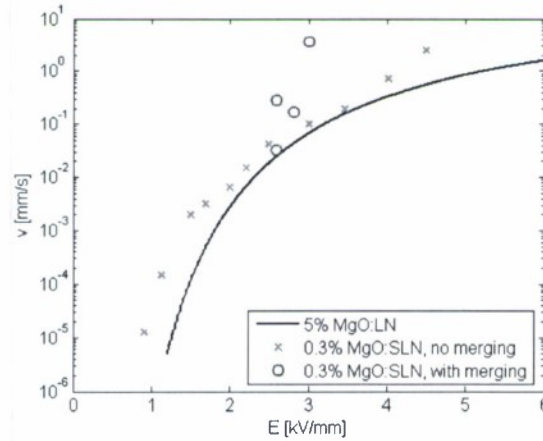

Figure 5: Domain wall velocity versus applied field for 0.3% MgO:SLN. The black curve is the corresponding dependence for 5% MgO:LN (Nakamura et al, J. Appl. Phys. **91**, 4528 (2002)).
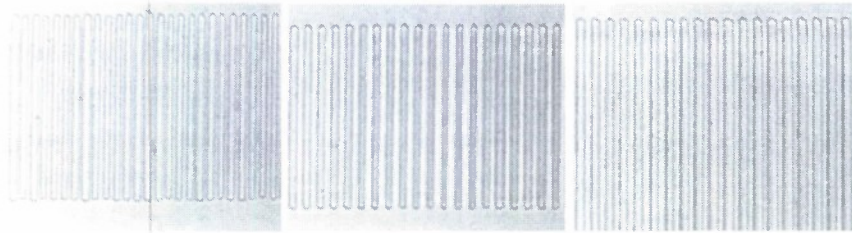

Figure 6: Periodic poling of VTE MgO:SLN for visible light generation. Left: 0.3% MgO:SLN, period=7 μm. Center: 0.3% MgO:SLN, period=9.6 μm. Right: 0.5% MgO:SLN, period=9.6 μm.

II.1.3 Waveguide Technology

Amplitude-modulation of QPM gratings (J. Huang)

The shape of the tuning curve of a frequency conversion device is most important in optical communications, where crosstalk is of great concern. As a result of the existence of tuning curve side-lobes, data channels whose wavelengths correspond to the side peaks will be converted and introduce crosstalk in WDM and TDM applications. The intrinsic sinc-square tuning curve of a uniform grating is typically unsatisfactory in that the ratio between its first side peak and main peak is only –13 dB, and its side-lobes decay only

quadratically with detuning. A side-lobe-free tuning curve is most desirable. Fourier transform analysis shows that the tuning curve side-lobes can be suppressed if the grating is apodized, i.e. the hard edges of the spatial nonlinearity profile removed. This requires amplitude modulation of a QPM grating.

With this motivation, we developed various techniques for amplitude modulation of QPM gratings in PPLN waveguides, as illustrated in fig. 7. The mode-overlap-control devices modulate the overlap integral of the waveguide mode with QPM gratings. The double-coupler structure effectively modulates the QPM processes in a waveguide by modulating the fundamental power along propagation. The deleted-reversal devices match the nonlinear coefficient distribution to an analog target function by deleting reversals in a deterministic way. By successful apodization, the side-lobes of the frequency tuning curves are suppressed by 13 dB or more, to approximately. −30 dB contrast, consistent with theoretical predictions as shown in fig. 8. In a wider context, these amplitude modulation techniques are not limited to apodization, but can be used for many other applications that require the alteration of tuning curve shapes.
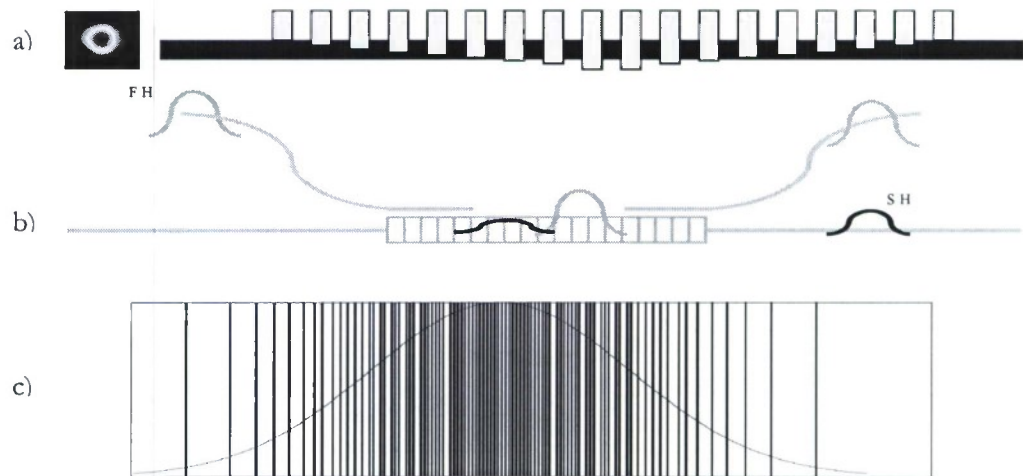

Figure 7: The three amplitude modulation techniques, from top to bottom: a) the mode-overlap control, b) the double-coupler structure, and c) the deleted reversals.
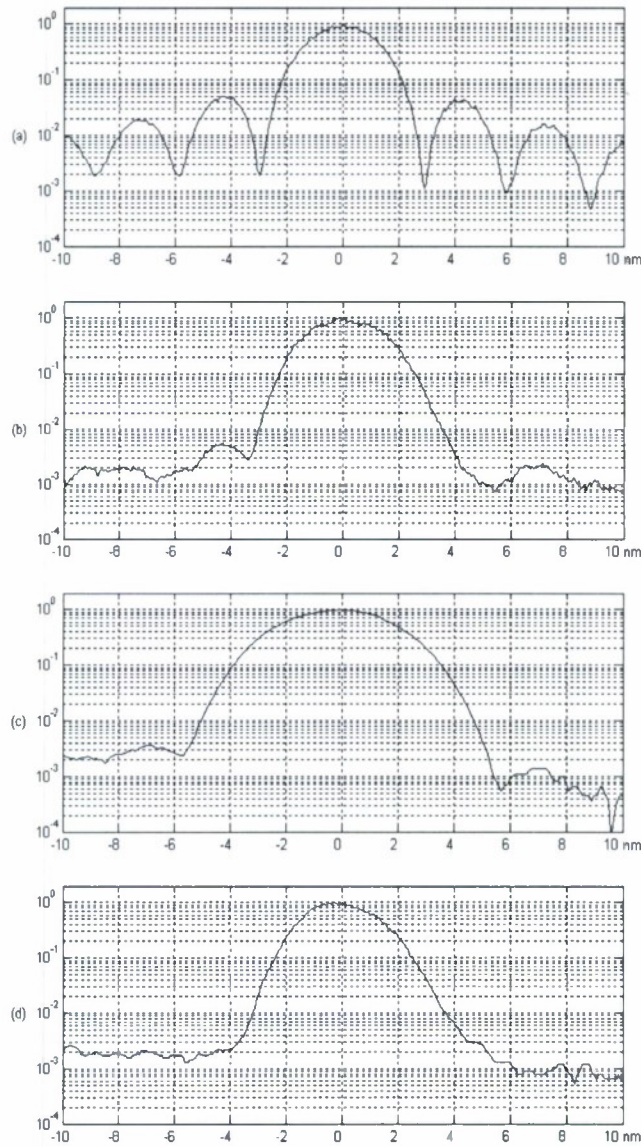
Figure 8: The normalized SHG tuning curves of a uniform grating and three apodized gratings, using each of the three apodization techniques above. The side-lobes have been clearly suppressed by apodization in each case.

Planar waveguides in VTE-MgO:SLN (R. Roussev)

Annealed proton exchange and reverse proton exchanged waveguides in 0.3 to 0.5% MgO:SLN are expected to provide both high conversion efficiency and adequate resistance to photorefractive damage. These properties would enable practical room-temperature waveguide devices for nonlinear optical signal processing, and possibly for green and blue light SHG. Proton diffusion studies were initiated in 0.3 and 0.5% VTE-MgO:SLN. The studies involved proton-exchange and multiple high-temperature anneals of planar waveguides. After every annealing treatment, the mode spectra of the waveguides were measured using a prism coupler. The mode spectra were then used for developing a model for the proton diffusion and

8

refractive index profiles of the waveguides. The model will be used for development and optimization of channel waveguide devices for frequency conversion in the near future

II.2 Devices

II.2.1 <u>Coherent</u> <u>Sources</u>

Generation of 589-nm yellow radiation by SHG (S. Sinha and D. Hum)

Recently, interest in generation of 589-nm radiation for adaptive optic and medical applications has increased. Astronomers using ground-based telescopes at visible and near-infrared wavelengths wish to use adaptive optic techniques to remove the atmospheric aberrations during observation. To correct for these abberations, a reference star positioned close to the observation star must provide enough light to a wavefront sensor. To provide a suitable reference, a laser can be used to excite a particular fluorescent species that sits atop the turbulent atmosphere. The wavefront distortion of the return radiation from the fluorescent species is then detected and corrected using a deformable mirror.

One of these techniques involves exciting the sodium layer which sits 90 km above the earth using 589-nm radiation. This laser guide star (LGS) system requires approximately 5 W of 589-nm radiation within a laser linewidth of 1 GHz (matched to the doppler broadened bandwidth of the sodium layer) to provide enough return light to the wavefront sensor for adequate performance. To meet these requirements, there are several possible sources at 589 nm. Currently, the best-developed solution is a simple dye laser which is pumped at 532 nm. Dye lasers are highly undesirable for astronomical telescope applications, however, because they are quite expensive to build and maintain, and the dyes themselves are often carcinogenic. Furthermore, the dyes are extremely flammable, forcing the need for expensive fire-proof enclosures.

Nonlinear optics may provide less-expensive and more-practical solutions to the LGS problem. Recently several schemes to produce 589-nm radiation from available solid-state and fiber sources have been proposed. Sum frequency generation from two Nd:YAG emission lines, 1.064 μm and 1.319 μm, has been used by Denman et al. (2006) to produce 50 W of 589-nm radiation in a doubly resonant cavity using lithium triborate (LBO) as the nonlinear optical element. Sum frequency generation from two fiber sources, the 938-nm line of Nd-doped silica glass and 1583-nm radiation from a Er-doped silica fiber have been summed by

Denman, C. et al., "Characteristics of sodium guidestars created by the 50-watt FASOR and first closed-loop AO results at the starfire optical range" Proc. of the SPIE, vol.6272, no.1, p.62721L-1-12(2006).

Dawson and co-workers at Lawrence Livermore (2005) using KTP and LT. Second harmonic generation from an 1178-nm Raman-amplified laser has produced 3 W of 589-nm radiation in melt-grown MgO-doped LT (Georgiev 2005). Finally, second harmonic generation using a 1178-nm bismuth doped fiber laser has been proposed.[Rukov 2007]. No matter what nonlinear interaction becomes the most efficient and inexpensive alternative, the nonlinear optical material can be chosen independently.

A set of periodically-poled devices with appropriate quasi-phasematching periods for SHG of 589-nm was fabricated. A 3.5-cm-long, 10.65-μm-period device was used in conjunction with an 1178-nm, Raman-amplified, master-oscillator power-amplifier system. Low power characterization of the device resulted in the temperature tuning curve that is shown in fig. 9. The tuning curve was not ideal, but fit well with a grating that was only 3.0 cm long. Merged domains toward the ends of the device can account for the discrepancy. The measured low-power conversion efficiency was 2 %/W, and is less than a factor of 2 below the theoretical efficiency of a 3.5-cm-long device.
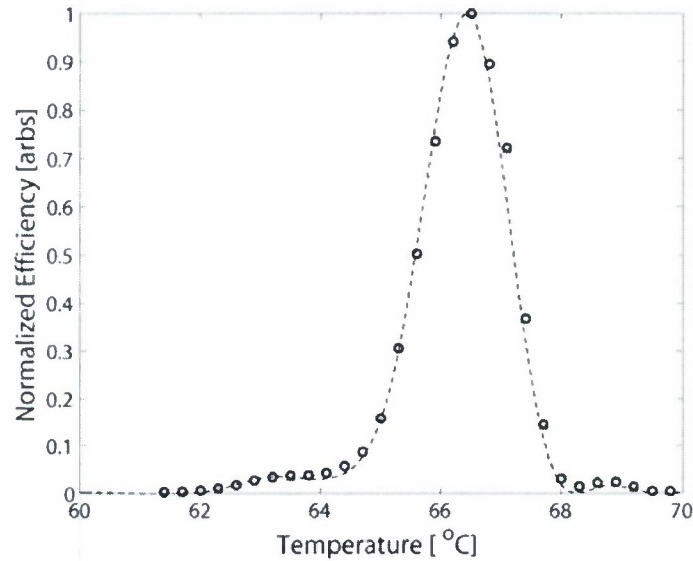
Figure 9: Temperature tuning curve for the generation of 589-nm radiation by SHG using a 3.5-cm-long, 11.65-μm grating. The open circles are measured data points and the solid curve is the theoretically expected tuning curve for a grating of only 3.0 cm long.

At higher powers, the Raman-amplified source broadened in linewidth which reduced the measured efficiency. As shown in fig. 10, the maximum output power reached 3.25 watts of 589-nm radiation from 20 W of 1178-nm radiation. The expected output for a source with the required 1-GHz-linewidth source would have been greater than 6 watts from 20 W of 1178-nm radiation. Unfortunately, the self-convolution of the electric field of the Raman-amplified source attained a linewidth in excess of 55 GHz which reduced the efficiency by a factor of 2. At the observed 3.25 W of 589-nm radiation, photorefraction and thermal limitations were not observed in the nonlinear device.

Dawson, J.W. with A. Drobshoff et. al., "469-nm fiber laser source" Proc. of the SPIE, vol.5709, no.1, p.193-8.

Georgiev, D. et. al., " Watts-level frequency doubling of a narrow line linearly polarized Raman fiber laser to 589 nm", Optics Express;; vol. 13, no.17 (Aug. 2005)

Rulkov, A.B. et.al., "6.4 W, narrow-line CW Bismuth-doped fiber laser for frequency doubling to 590 nm", CLEO '07. 2007 Conference on Lasers and Electro-Optics, 7, Baltimore, MD; p.2489-90 (5-11 May 2000)
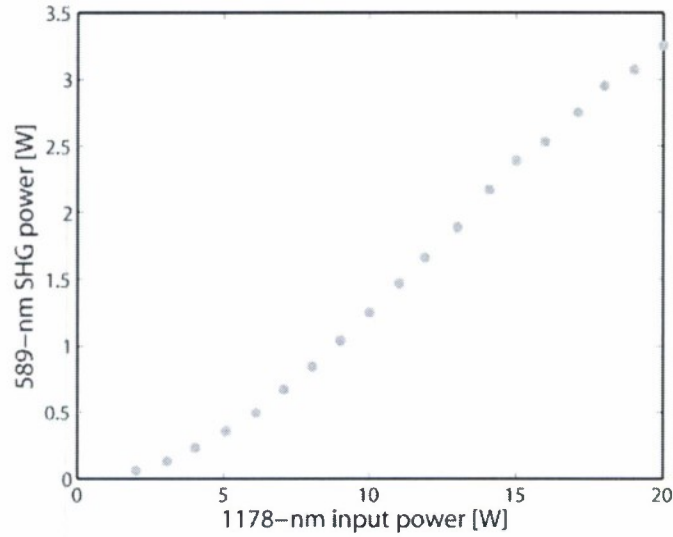
Figure 10: SHG power at 589 nm as a function of 1178-nm input power. The roll-off in efficiency is attributed to the dramatic increase in pump linewidth as a function of pump power, exceeding the QPM bandwidth of the crystal.

In collaboration with Lockheed Martin - Coherent Technologies, Inc., generation of 589-nm radiation by SFG was performed with a 36-mm-long sample. Using two 77-MHz-repetition-rate, mode-locked Nd:YAG lasers, 8.7 W of 589-nm radiation was produced with 16 W of 1064-nm radiation and 9.1 W of 1319-nm radiation. The pulse width of the 1064-nm laser was 0.6 ns and it was focused to a 43-μm spot (1/e2-intensity radius). The pulse width of the 1319-nm laser was 0.4 ns and was focused to a 50 μm spot (1/e2-intensity-radius). The optimum phasematching temperature was 80.9 °C for a quasi-phasematching period of 10.8 μm, and the sample showed no photorefractive damage at the maximum output power tested.

Generation of 458-nm radiation by SHG using stoichiometric lithium tantalate (D. Hum)

Argon-ion lasers have multiple emission lines including those located at 457.9 and 488 nm. To replace the argon-ion lasers with compact and efficient solid-state lasers that conveniently lase at wavelengths close to 915 nm (912 nm for Nd:GdVO$_4$ and 914 nm for Nd:YVO$_4$), efficient and robust nonlinear optical conversion devices that have long service lifetimes are required. Moreover, blue lasers with wavelengths ranging from 457 nm to 460 nm have garnered interest with application to laser display technology. To examine the feasibility of generation of shorter wavelengths, the feasibility of fabricating quasi-phasematching periods as short as 4.9 μm was investigated.

A tunable, CW, Ti:sapphire laser was used to generate wavelengths around 455 nm to 458.5 nm at or near room temperature. With 90 mW of pump power, a maximum power of 60 μW was produced internally. The conversion efficiency of 0.5 %/(Wcm) is approximately a factor of 2 from ideal for the 1.5-cm-long device for the focusing conditions used. The measured temperature tuning curve is shown in fig. 11 below. Photorefraction was not observed at these power levels; these devices should be examined at higher average and peak powers in future work to verify their apparent resistance to photorefractive damage and blue-induced infrared absorption.
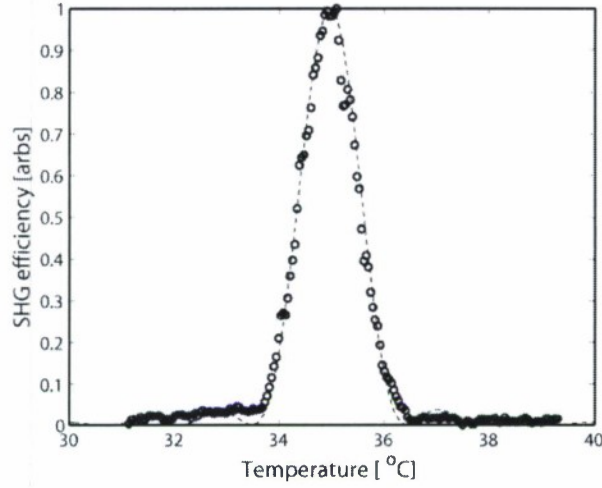
11

Figure 11: Temperature tuning curve of a 1.5-cm-long device generating 458.3 nm by SHG Measured data (circles) match well with the theoretical curve (dashed line).

Large aperture devices: Generation of 532-nm radiation by SHG using stoichiometric lithium tantalate (D. Hum)

The use of congruently melting periodically-poled (PP) lithium tantalate is limited to wafers on the order of 1 mm in thickness because of the high applied electric field, about 20 KV/mm, required for the periodic poling process. Without elliptical focusing of the laser beam, this thickness limitation restricts the available optical aperture to an area of approximately 1 mm². Previous efforts to increase the useful aperture of periodically-poled (PP) ferroelectrics have included the use of thick substrates (~5 mm) of lower coercive field ferroelectrics such as magnesium-oxide-doped lithium niobate, and diffusion bonding of un-poled lithium niobate wafers to PP lithium niobate wafers, which effectively buries the PP section in a larger cross-section of non-periodically-poled material having the same optical indices.

In this section, we discuss this challenge and its solution in the use of periodically poled, near-stoichiometric, lithium tantalate (PPSLT). Previously, we proposed a topology for a scalable crystal aperture based on periodic poling of a rotated-cut ferroelectric wafer [Hum]. This topology is illustrated in fig. 12a below.
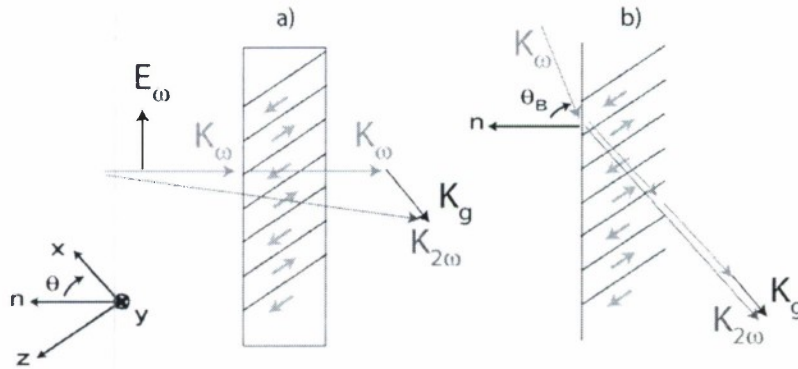

Figure 12: a) Topology for large aperture periodically poled crystals. Light propagates through the large wafer face with a component of the electric field polarized along the z-axis, thus enabling efficient second harmonic generation (SHG) in addition to other nonlinear interactions. b) For 25-degree-rotated (θ=25°), X-cut substrates, light incident at near Brewster's angle, θB, allows a collinear SHG interaction.

12

Light incident on the large wafer surface can be polarized with a component along the extraordinary-axis to use the largest nonlinear coefficient and make use of a geometrical projection of the propagation vector onto the QPM grating k-vector. Previous results of periodic poling of rotated-cut substrates were carried out on wafers oriented for surface acoustic wave (SAW) applications.

For nonlinear optics purposes, we chose to develop periodic poling of 25-degree-rotated, X-cut, near-stoichiometric lithium tantalate wafers that had been processed by vapor transport equilibration (VTE). The 25-degree angle of rotation allows light incident near Brewster's angle to propagate normal to domain walls containing the z-axis and hence allows – collinear interactions, taking advantage of the largest component of the nonlinear susceptibility tensor. This particular SHG orientation is illustrated in fig. 12b. The cut of the crystal indicates that the alternate ordinary axis is in the plane of the wafer. We chose to force the y-axis to be in-plane since +y and –y domains have different etch rates. This differential etch rate permits us to visualize domains by etching and observing the sides of the wafers after periodic poling..

Near-stoichiometeric lithium tantalate (SLT) is free of photorefractive damage (PRD) and green-induced infrared absorption (GRIIRA). Most commercially available lithium tantalate is congruently-melting and contains 48.39 mol% lithium oxide, whereas crystals of near-stoichiometric composition have compositions close to 49.95 mol% lithium oxide. The lithium deficiency of congruently melting lithium tantalate causes native defects that are widely accepted to be one tantalum anti-site defect and four lithium vacancies. The concentration of native Ta anti-site defects closely correlates with the magnitude of PRD and GRIIRA and to the magnitude of the ferroelectric coercive field. Thus, SLT has reduced sensitivity to PRD and GRIIRA and has lower coercive field. We have chosen to produce our SLT by the vapor- transport-equilibration method. The VTE method produces crystals with a coercive field as low as 100 V/mm, consistent with a composition of 49.99 mol %.

The original substrates for the VTE process were SAW-grade, 50-mm-diameter, 1-mm-thick, 25-degree-rotated, X-cut CLT wafers from Sawyer Technical Materials, LLC. The VTE process was carried out at 1360 °C for 120 hours. After the VTE processing, it was necessary to uniformly pole the SLT crystals before reproducible periodical poling was possible. The uniform poling process was performed at 185 °C with graphite electrodes and applied fields as high as 1000 V/mm to remove the head-to-head domains that result from the VTE process. To ensure complete polarization, the applied field was reversed several times. Afterwards, the crystals were annealed in air at 620 °C for 10 hours.

At room temperature, the "apparent" coercive field (the applied voltage divided by the wafer thickness) and the spontaneous polarization (the charge per unit area transferred in tracing a complete hysteresis loop) were 315 V/mm and 27 $\mu C/cm^2$, respectively.

For rotated-cut materials, the apparent coercive field and the spontaneous polarization are the conventional z-cut coercive field and spontaneous polarization scaled by the geometric projection of the surface normal onto the z-axis for the crystal. Projecting this field and the spontaneous polarization onto the direction of the ferroelectric axis yields 133 V/mm and 63 $\mu C/cm^2$, respectively, which is consistent with the values we got with similarly processed z-cut substrates. Before periodic poling, the crystals were ground and polished on both sides to a final dimension of 0.5 mm in thickness. Periodic poling was carried out at 120 °C with aluminum electrodes evaporated over a photoresist pattern. The reduced thickness and elevated periodic poling temperature served to increase nucleation and improve overall domain quality. Poling was performed with a single poling pulse of 15 ms duration at 540 V/mm to produce gratings with a period of 8 μm for first-order QPM SHG of 532-nm radiation. Samples were then polished along the +y surface and chemically etched for 20 minutes to reveal the domain patterns. A photograph of a chemically etched sample is shown in the inset of fig. 13. After periodic poling and etching, the aluminum electrodes and photoresist were removed for SHG measurements.
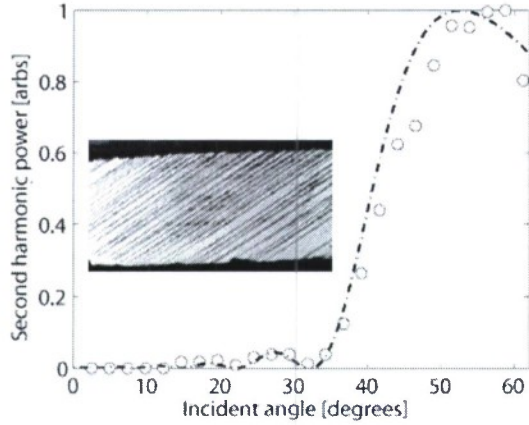
Figure 13: An angular tuning curve of SHG power as a function of incident fundamental angle The dotted curve represents the theoretical angular tuning curve. (Inset) Photograph of 25-degree-rotated domains (+y surface) revealed by chemical etching in hydrofluoric acid The domain period is 8 μm.

To examine the local efficiency and the high-energy operation of the substrates, two separate SHG measurements were performed. A modelocked, 9.2-W average-power, 7-ps, 50-Mhz repetition-rate, 1064-nm laser was loosely focused to a 135 μm spot ($1/e^2$-intensity-radius, excluding the foreshortening due to non-normal incidence on the sample). An angle-tuning curve was measured and it fit well with the theoretical calculations. The generated SHG power was then measured as a function of position over a 6 mm by 7 mm area on a right-angle triangular sample, 15 mm by 15 mm in size. The results from this experiment are shown in fig. 14. The maximum SHG power generated was 30 mW, which is a factor of 3.5 below the theoretical for the loose focus condition. The discrepancy can be explained by poling errors (mostly merged domains) and domains that did not propagate the full thickness of the wafer. The laser was then focused to a 30-μm spot ($1/e^2$-intensity-radius, excluding the foreshortening) and generated a maximum of 540 mW of 532-nm radiation. The experimental conversion efficiency is again a factor of 3.5 below theoretical. Although the uniformity of the sample was poor, further improvements in periodic poling should enable scaling of the useable area for future devices.
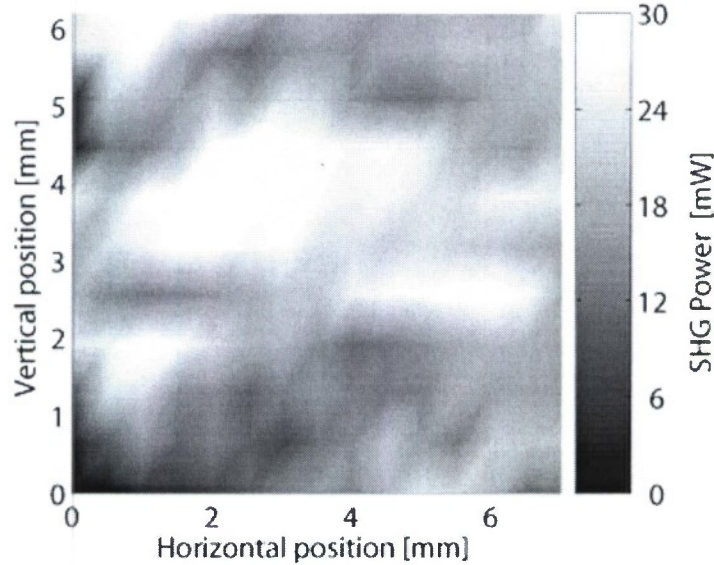

Figure 14: Spatial map of the generated 532-nm power as a function of position.

To examine the high-energy capacity of a rotated cut sample, we focused a 1.0-J-per-pulse, 7-ns, Q-switched, 1064-nm laser on a 0.26-cm² area of the crystal (including the foreshortening). The damage threshold in z-cut near-stoichiometric tantalate fabricated by vapor transport equilibration was measured to be 7.3 J/cm² for

14

12 ns pulses. At the input energy of 1.0 J, no laser-induced damage was observed and the SHG energy was measured to be 21 mJ, a factor of 4.2 below theoretical.

In summary, we demonstrated a large-area, scalable QPM nonlinear device based on 25-degree-rotated, X-cut, near-stoichiometric lithium tantalate fabricated by VTE. The device operates at near Brewster's angle with an efficiency of nearly 30% of the theoretical value in the ps regime, and it has been shown to support 1.0 J of pulse energy at 1064 nm. With further improvement of the periodic poling quality and the use of optical quality crystals, we believe that 50 % efficient conversion is possible out to a pulse width of 7 ns.

> *Generation of 19 Watts of single-frequency 532-nm ratdiation in stoichiometric lithium tantalite (S. Sinha and D. Hum)*

This section describes a system that produced 19 W of diffraction-limited radiation at 532 nm through single-pass frequency doubling of the output of a 1064-nm Yb^{3+}-doped fiber MOPA in a periodically-poled, near-stoichiometric lithium tantalate (PPSLT) crystal. The output of the system was stable at the 19-W level for over one hour with no signs of photo-refraction. The green power is believed to be limited by infrared-induced thermal de-phasing in the PPSLT crystal.

Because of their high nonlinearities and resistance to photorefractive refractive damage and photo-chromic effects, such as green-induced infrared absorption (GRIIRA), stoichiometric ferroelectrics are ideally suited for the 100-W and kW range powers that have now become available from fiber laser systems. The development of these stoichiometric nonlinear materials coupled with efficient fiber laser systems has led to the demonstration of efficient narrow-linewidth, watt-class sources in the green and yellow. We describe here a system that generates 18.8 W of cw diffraction-limited power at 532 nm in a single longitudinal mode through frequency doubling the output of a Yb^{3+}-doped fiber MOPA in a periodically poled near-stoichiometric lithium tantalate chip. To the best of our knowledge, this power represents the highest diffraction-limited power in the green (cw or average) that has been generated in a periodically poled material. It is also the highest cw power generated through nonlinear frequency conversion to the green in a single-pass configuration (QPM or birefringently phase matched).

Optical frequency doubling of a narrow-linewidth, 1064-nm source was performed in a 4-cm-long, 1-mm-thick PPSLT sample. The pump source was a Yb^{3+}-doped fiber amplifier seeded by a 2-W single-frequency 1064-nm Nd:YAG non-planar ring oscillator (NPRO) with a measured FWHM linewidth of 10 kHz. The amplifier consisted of a commercial polarization-maintaining double-clad silica fiber from Nufern with a 20-μm, 0.06-numerical aperture (NA) core and a 400-μm-diameter 0.44 NA inner cladding and a stress-induced birefringence in the core of 3.7×10^{-4}. The amplifier produced a maximum output power of 136 W with an optical efficiency of 56% with respect to incident pump power. The near-stoichiometric lithium tantalate was produced from a commercial congruent composition wafer and subjecting it to the VTE process. After the VTE process, the wafer was lithographically patterned and periodically poled by the electric field poling method referred to previously. A low-temperature broadband anti-reflection (AR) coating with a center wavelength of approximately 800 nm was applied to both ends of the chip to maximize the output power in the green. The PPSLT chip was placed in a custom mount whose temperature was controlled with a thermo-electric cooler (TEC) and monitored with a thermistor.

We measured a low-power, normalized conversion efficiency of 0.3%/(W·cm) in our PPSLT chip, which is about 2.2 times lower than ideal given our focusing conditions. The discrepancy was most likely caused by a non-ideal poling duty cycle. To demonstrate that these PPSLT frequency doublers could be operated near room temperature without the onset of photorefractive damage, gratings with a poling period of 8.0 μm that were designed to phase-match the 1064-nm frequency doubling process at 40°C were used. Low-temperature phase-matching has the additional advantage that the thermal conductivity of SLT is higher at lower temperatures, so the temperature rise is reduced for a given amount of absorbed optical power. As a result of

the tilt of the chip, the peak phase-matching temperature was shifted downwards to 31.3°C. As shown in fig. 15, the measured low-temperature tuning curve for the 4-cm device agrees well with theoretical predictions.
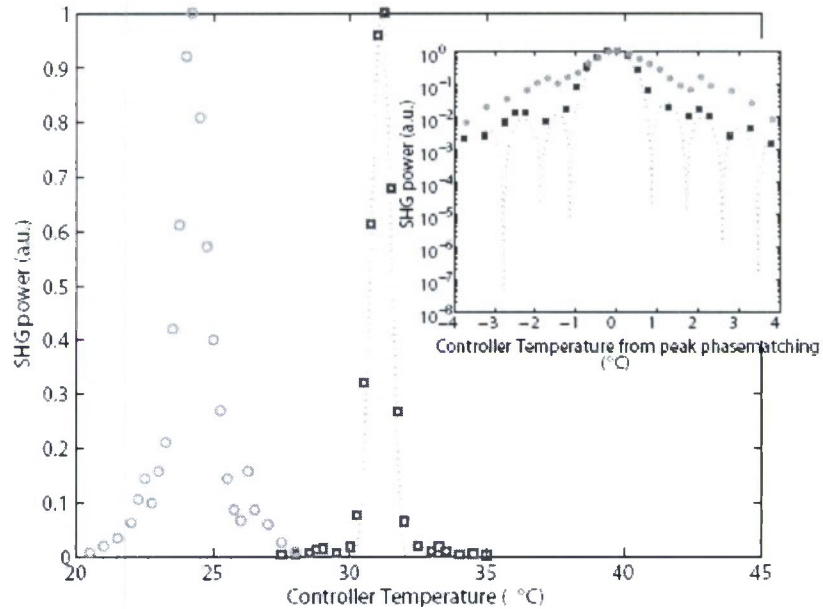

Figure 15: Temperature tuning curves for the PPSLT chip. The low-power measurements (squares) and the theoretical tuning curve assuming no absorption (dotted line) for the given focusing conditions are shown. The measured tuning curve at the 19-W level is also shown (circles). Inset: Superimposed tuning curves at low-power (squares) and high-power (circles) on a logarithmic scale. The theoretical curve (dotted line) is also shown.
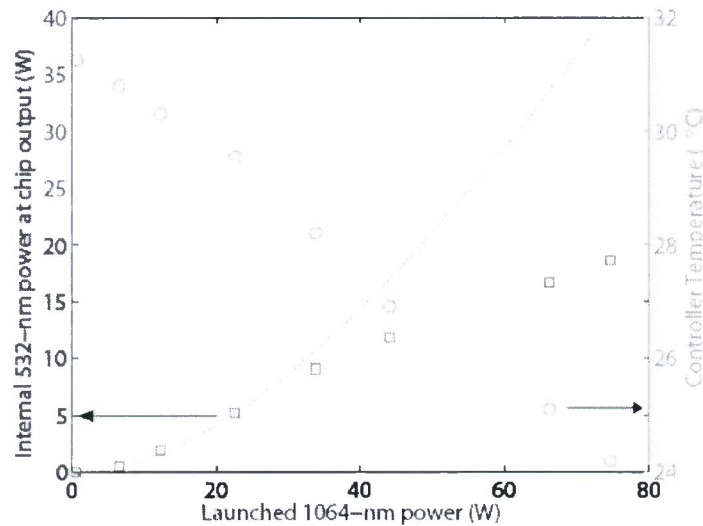
Figure 16: Internal SHG power (squares) and optimum controller set-point temperature (circle) versus internal 1064-nm power. The dotted line is the extrapolated P×tanh² curve from the measured low-power conversion efficiency.

21

We increased the power from the fiber amplifier incident on the PPSLT chip in steps and monitored the generated green power as shown in fig. 16. As the 1064-nm power was increased, the controller's temperature set-point for the PPSLT chip was manually adjusted to maintain maximum green power. The need for the adjustment was due predominantly to absorption of the incident IR in the PPSLT chip. We measure a maximum power of 18.3 W outside of the chip (corresponding to 18.8 W inside the chip) with a launched 1064-nm power of 75 W. This represented an overall optical efficiency of 16% with respect to incident diode pump power. As the incident fundamental power was increased beyond 30 W, we found that the generated green power began to deviate from the theoretical $\tanh^2$ curve. We think that this deviation may have been due to thermal de-phasing, a process by which the phase-matching in the nonlinear medium is spoiled due to the uncompensated temperature dependence of the refractive index at the fundamental and second harmonic frequencies.

At the maximum green power observed, 18.8 W, the temperature tuning curve shown earlier in fig. 15 was measured as well. The broadening of the tuning curve at maximum power is clearly illustrated in the inset, in which the low-power and high-power tuning curves have been superimposed on semi-logarithmic axes.

The beam quality of the IR and green beams were each measured at both low and high power. At low powers, the M2 of the IR beam was found to be 1.05 and 1.03 in the horizontal and vertical dimensions, respectively. At the maximum used power of 75 W, the M2 of the 1064-nm beam was 1.04 and 1.05 in the horizontal and vertical dimensions, respectively. At low powers, the M2 of the 532-nm beam was 1.04 and 1.01 in the horizontal and vertical dimensions, respectively. At the maximum power of 18.8 W, the M2 of the green had deteriorated slightly to 1.19 and 1.05 in the horizontal and vertical dimensions, respectively, probably due to thermal focusing.

II.2.2 Broadband and Ultrafast Nonlinear Devices

Ultra-broadband Parametric Amplification and Engineering of the Gain Spectrum (M. Charbonneau-Lefort)

Optical parametric interactions have emerged as a convenient way of amplifying short pulses. In that context, quasi-phase-matching (QPM) has opened the door to new possibilities. Among them is the engineering of nearly arbitrary phase-matching profiles. For one thing, chirped QPM gratings provide a way of phase-matching a broad, continuous range of frequencies in a single device and thus constitute a promising candidate for ultra-short pulse amplifiers. But the capabilities offered by non-uniform phase-matching profiles go much further: non-uniform QPM gratings can in fact be designed to yield the prescribed gain and group delay spectra.

The purpose of our work in this area was to explore the possibilities offered by non-uniform QPM gratings, for applications as ultra-short optical pulse amplifiers. In particular, our goal was to understand how to design optical parametric amplifiers (OPAs) offering desired gain and group delay spectra.

We developed a method of analysis flexible enough to be applicable to a wide variety of cases but which offered sufficient simplicity to allow the design of new devices. With these theoretical tools we were able to explore the design space of OPAs using non-uniform phase-matching media, and formulated "design rules" for the fabrication of such devices.

As a matter of illustration we consider a few examples. In the case of a linear profile, the amplification spectrum is essentially uniform over a wide bandwidth (see Figure 17a). The ripple can be reduced by turning on the interaction adiabatically, either by tapering the coupling coefficient or by modifying the profile so that the wavenumber mismatch becomes very large at the edges of the grating, as shown in fig. 17b. Alternatively,

by varying the chirp rate one can obtain almost any smooth gain profile. For instance, introducing a sinusoidal modulation to the linear profile yields an amplification spectrum consisting in a number of "peaks", or amplification bands, as shown in fig. 17c.
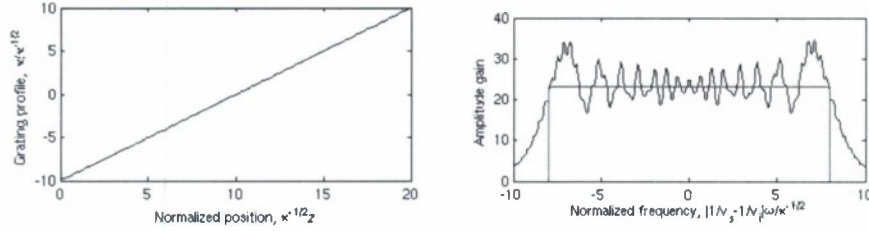

Figure 17a: Linear QPM grating profile (left) and the corresponding amplification spectrum (right).
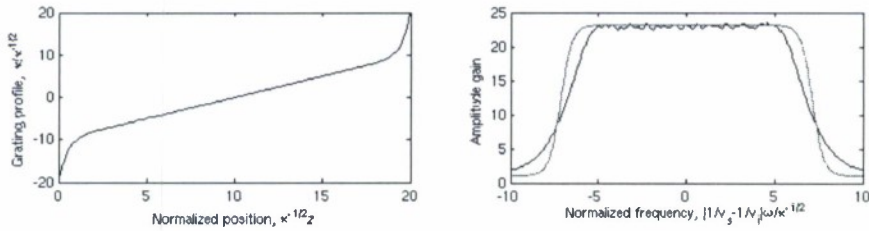

Figure 17b: Profile for ripple reduction, with large wavenumber mismatch at the edges of the grating (left) leading to an amplification spectrum with significantly reduced ripple (right).
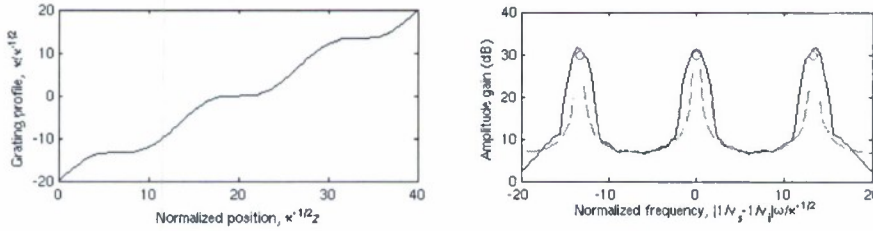
Figure 17c: Linear grating profile with sinusoidal modulation (left). The corresponding amplification spectrum presents amplification peaks useful for selective frequency amplification (right).

Finally, it is important to keep in mind that the amplification of ultrashort optical pulses requires tight control of the phase. To this end we have proposed a design which allows us to specify at the same time the gain and the group delay spectra, using a pair of gratings in a tandem configuration as illustrated in fig. 18. The details of this design were published in Optics Letters 30, 634 (2005).
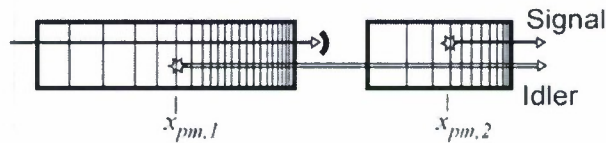

Figure 18: OPA using tandem chirped QPM grating for simultaneous gain and group-delay control.

An experiment was carried out to confirm our theoretical model. The experimental setup is shown in fig. 19. We use a Q-switched Nd:YAG laser as the pump beam and a diode laser tunable around 1550 nm as the

23

input signal. Both beams are combined and focused into a crystal of periodically-poled lithium niobate. Each nonlinear crystal contains several gratings of various phase-matching periods and chirp rates.
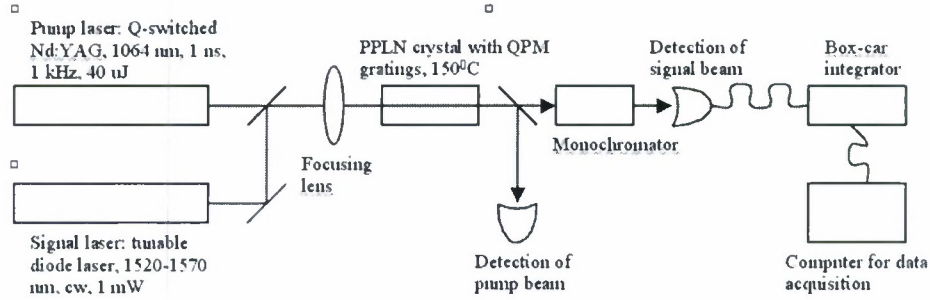

Figure 19: Experimental setup for the measurement of the amplification spectrum of non-uniform QPM gratings

The experiment showed that chirped QPM gratings yield a constant gain over a wide bandwidth, as expected. However, it also revealed the existence of two unexpected high-gain processes. First, there exist laterally-confined gain-guided modes which can be seeded at a non-collinear angle. If the angle is too shallow, growth is impossible because the chirp of the QPM grating limits the amplification to the phase-matched region. If the angle is large enough, the waves escape the pump beam before experiencing significant dephasing, and gain-guided modes can exist. However, if the angle is too large, these modes cannot grow because the gain is insufficient. Therefore, there is a range of non-collinear angles where gain-guided non-collinear modes exist. In practice, these non-collinear interactions can be seeded by "quantum noise" and lead to a relatively intense parametric fluorescence emission.

These modes were discovered in uniform phase-matching media by Sushchik [Suschchick and Freidman, Radiophysics & Quantum Electronics 13, 1043 (1970)]. In the course of our work, we have found the generalization of the Sushchik modes to the case of non-uniform phase-matching media (in our case, chirped QPM gratings).

The second unexpected result revealed by our experiment is the difference between the behavior of positive and negative chirp rates. When the chirp rate is positive, the amplification is localized in the vicinity of the phase-matched point. This is the desired behavior of a chirped QPM grating. However, when the chirp rate is negative, the phase accumulation caused by diffraction can be cancelled by the phase de-accumulation due to the negative chirp rate. This results in amplification over the remaining length of the device, leading to large variations of the gain from one end of the amplification spectrum to the other.

As far as broadband optical parametric amplifiers are concerned, these two effects (namely, the existence of non-collinear gain-guided modes and the amplification resulting from the balance between diffraction and negative phase accumulation) are undesired. Their impact can be reduced by using a sufficiently wide pump beam. Practical design criteria have been formulated for publication.

Ultra-broadband optical parametric generation (OPG) (P.S. Kuo)

In related work on another engineerable nonlinear optical material, orientation-patterned GaAs (OP-GaAs), supported under AFOSR MURI Grant F49620-01-1-0428, we recently demonstrated optical parametric generation (OPG) of ultra-broad mid-infrared output from 4.5 to 10.7μm (measured 20dB down from the peak). The OPG spectrum for 3.28-μm pump wavelength at 1.4-μJ incident energy is plotted in fig. 20.
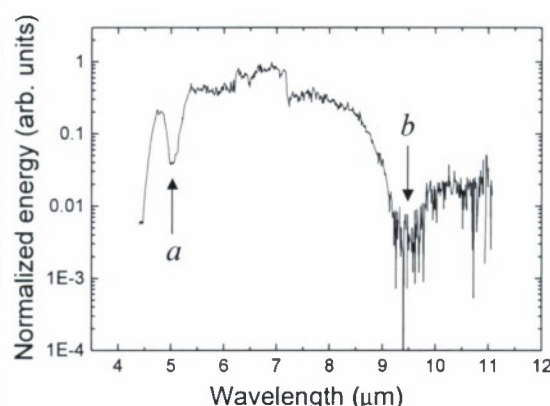
24

Figure 20. OPG output spectrum for 3.28µm pump at 1.4µJ energy. Dips at 5 and 9.5 µm (marked *a* and *b*, respectively) are due to parasitic SFG.

We believe this ultra-broad infrared spectrum is an interesting ultrafast, near-diffraction-limited "light bulb" source for various spectroscopic applications where octave bandwidths combined with tight focusing or high degree of collimation are required.

II.2.3.Bulk Nonlinear Devices

Near-stoichiometric MgO:Lithium Niobate (R. Roussev)

During the previous reporting period, SHG of 1.3 W of green light was demonstrated in 0.3 mol-%MgO-doped near-stoichiometric lithium niobate (MgO:SLN) that was prepared by vapor-transport equilibration (VTE). In that experiment, the green power level was limited by the available fundamental pump power and the relatively low quality of periodic poling.

In this current reporting interval, the process of periodic poling 0.3-mol-% MgO:SLN was further optimized to achieve QPM gratings of very good quality with periods suitable for SHG of green light. Experiments on frequency doubling of 1064-nm radiation from an Nd:YAG laser were performed with two periodically poled MgO:SLN crystals, 17 and 12-mm long, respectively. The thickness of the crystals was 0.26 mm. The pump laser radiation was launched as an e-polarized wave for type I phase-matching using the d_{33} nonlinear coefficient. Based on the Sellmeier equation of MgO:SLN determined in the earlier stages of this program, phase-matching was expected to occur at room temperature for a QPM period of 7.09 µm. The experimentally observed phase-matching temperature was 18 °C for a QPM period of 7.08 µm and 28 °C for a period of 7.6 µm.

In the 17-mm-long crystal, as the CW pump power was gradually increased, stable operation at green power levels reaching 3 W inside the crystal was observed. At a green power level of 3.4 W, the crystal output facet cracked. The cracking occurred after the phase-matching temperature was adjusted for maximum green power, not during the increasing of the fundamental pump power. The trace of the crack appeared to be caused by thermal self-focusing. The local heating seemed to be due to absorption related to the green beam, since no damage was observed at the full 14 W of pump without high-intensity green light (e.g., at crystal temperatures away from phase-matching).

With the shorter crystal, an input lens with shorter focal length was used, to ensure that the beam focusing was near optimum (the crystal length being between 2 and 5.6 times the confocal parameter). In this case, the lower-power results were recorded before the crystal cracked. The results of green output power versus laser

power are shown in fig. 21. The green power was stable at all pump power levels up to the point of crystal cracking.
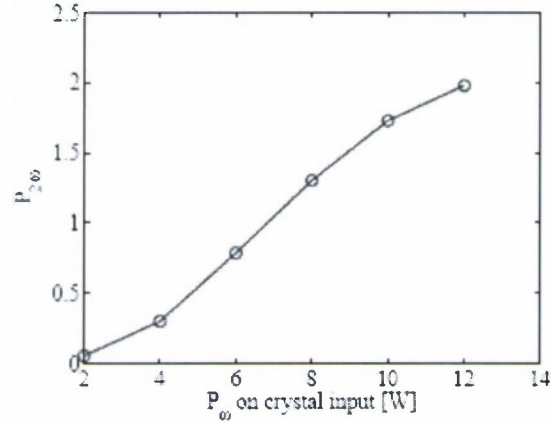

Figure 21 Green power generated in the 12-mm MgO:SLN crystal versus input pump power at 1064 nm

There is clear deviation from the quadratic dependence characteristic for SHG in the low-conversion limit. At the maximum green power of 2 W, only about 20% of the pump power in the crystal has been converted to green. Therefore, most of the deviation from the quadratic dependence is due to thermal dephasing, causing non-uniform QPM along the beam. After stable generation of 2-W of 532-nm radiation for 4 hours, the pump power was increased from 12 to 14 W. The crystal temperature had to be reduced to compensate for the local heating caused by the laser beam. As soon as the green power level reached ~2.5 W, the crystal cracked.

From the above experiments, it is clear that the maximum power in the crystal is limited by absorption related to the green intensity. The absorption may be either absorption of the green itself, or GRIIRA. The saturated space-charge field of the substrate, from which the crystals were cut, was 10 V/mm. Although this value is low enough to avoid significant PRD, it is larger than the lowest values of ~1 V/mm, obtained for 0.3 mol-% MgO:SLN. This indicates that there may be some residual antisites. Therefore, some residual GRIIRA may be present. Further studies should focus on experiments with samples with lower space- charge field that presumably have smaller GRIIRA. In addition, measurements of GRIIRA and green absorption should clarify which of the two was larger at green power levels of 2.5–3.5 W and residual pump in the crystal of 6.5-7.5 W. Reduction of the absorption in the green part of the spectrum may be possible with longer annealing in air, annealing in oxygen, or electrochemical oxidization of the crystal.

II.2.4 Waveguide Nonlinear Devices

Mid-infrared generation by difference-frequency mixing in a PPLN waveguide (R. Roussev)

In the previous period, efficient tunable generation of narrow-line mid-infrared radiation near 4060 nm via difference-frequency mixing in a periodically-poled waveguide was demonstrated. Conversion efficiency of order 20%/W was observed from a device with 4.6-cm long QPM grating. Due to the low-power pump at 1119 nm, only microwatt-level mid-IR signal was generated. The waveguides were fabricated in regular congruent lithium niobate.

During the recent period, our efforts focused on estimating the losses at the mid-infrared wavelength, as well as exploring the possibilities for higher mid-infrared power by pumping with more powerful pump at 1119 nm. The mid-infrared radiation was generated by using a tunable input signal near 1550 nm. The losses at the signal were ~0.1 dB/cm, measured by the Fabry-Perot method. The losses at the mid-IR were

26

measured by comparing the mid-IR output identical waveguides with short QPM gratings located at different positions along the waveguides. The losses were found to be 0.7 +/- 0.2 dB/cm for reverse-proton exchanged waveguides on one PPLN chip, and 1.2+/- 0.2 dB/cm on another. The following conclusions can be made:

1. The losses in the mid-IR are significantly higher than the losses near 1.55 μm.

2. The higher losses in the second chip correlate with a slightly higher peak proton concentration. The estimated peak concentration in the second chip was in the range ~0.21–0.22, while it was ~0.20–0.21 in the chip with lower mid-IR losses.

3. The higher losses in the second chip also correlate with a slightly shallower waveguide depth. The waveguides in the lower-loss chip were buried slightly deeper with the longer RPE. The difference is small, though, and not likely to cause a significant difference in propagation losses. So far, no special experiments have been performed to determine whether losses due to surface scattering have a major contribution in the observed high losses in the mid-IR.

Waveguides from the lower-loss chip were used for DFG mixing efficiency measurements using the same pair of lasers described above. The observed efficiency range was 12-25%/W-cm² for waveguide widths between 15 and 21 μm. The measurement error was comparable to the difference in efficiency between different devices. The efficiency was highest for the waveguides with widths of 16 and 17 μm, where the non-critical width was located.

A waveguide with a width of 14 μm and a full-length QPM section was used for generation of mW-level mid-IR radiation. In order to obtain high mid-IR power, the output of the 1119.1-nm pump laser was passed through a fiber amplifier, delivering up to 160 mW of output power. The dependence of DFG-output power on signal power coupled in the waveguide with a fixed pump of 114 mW inside the waveguide is plotted in fig. 22. The observed efficiency is ~6%/W. The linear relation between signal and idler, characteristic for the low-conversion regime, is confirmed. At the maximum DFG power of 5.7 mW, over 20 mW of pump had been converted to signal and idler.
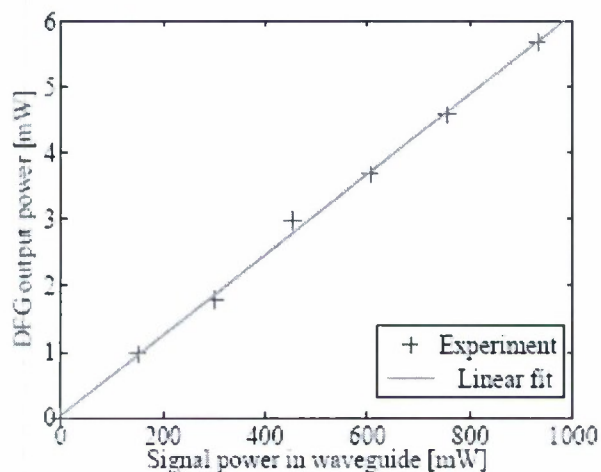

Figure 22: DFG power versus signal power for a pump power of 114 mW coupled in the waveguide

With pump power near 100 mW and several hundred milliwatts of signal, some red, green and orange light was observed on the output of the waveguide due to parasitic SHG of the signal, SHG of the pump, and SFG between the pump and the signal, respectively. These small amounts of visible parasitic light caused observable shifting and distortion of the QPM tuning curve at room temperature presumably due to the photorefractive effect. The measurement time was limited to 10-20 seconds per point, to avoid significant photorefractive damage to the waveguide.

To observe higher DFG output power, the power of the pump laser was briefly increased 239 mW by heating the fiber amplifier and increasing the current of its pump diodes. With ~170 mW of coupled pump power and ~900 mW of signal, 8.1 mW were generated at 4 μm.

The observed efficiency in the high-power experiments was 2–4 times smaller than the efficiency estimated during the preliminary measurements without the fiber amplifier at the pump wavelength. The main reason for the discrepancy is multimode pump coupling in the high-power experiment. The low-power experiments were performed using a different fiber collimator for the pump beam and a different focusing lens on the waveguide input, producing a smaller pump spot-size. During the high-power experiments, the pump exiting the PPLN waveguide appeared multimode. The mid-IR power can be increased two to three fold with proper coupling into the fundamental mode.

Similar experiments were performed for the generation of mid-IR radiation with a wavelength in the range 3.2-3.45 μm. The waveguide chip (C4) contained channel devices with widths ranging from 14 to 20 μm, QPM periods of 25.65, 25.80 and 25.95 μm. Using a 1064-nm laser as the pump and an amplified tunable diode laser near 1550 nm as the signal, DFG near 3.3 μm was explored. The observed efficiency was lower than that near 4 μm, opposite to the wavelength scaling derived from mode-overlap calculations. The difference is attributed to propagation losses in the mid-IR, which increase as the DFG output wavelength approaches the OH^- absorption peak near 2860 nm. By comparing the theoretical expectations with the experimental efficiencies, the losses at 3.3 μm were estimated to be ~6 dB/cm.

For high DFG power, pump powers of several hundred milliwatts were coupled in a waveguide. In order to reduce photorefractive effects, the experiments were performed at 70 °C. The signal phase matching wavelength was ~1543 nm for a QPM period of 25.80 μm and ~1567 nm for a QPM period of 25.95 μm. The corresponding mid-IR idler wavelengths were 3.43 and 3.31 μm, respectively. The efficiency at elevated temperatures was smaller compared to room temperature, and the tuning curves were wider. This was attributed to increased propagation losses, since the tuning curves appeared Lorentzian, which is typical in the loss-limited regime. In addition, the normalized efficiency of generation of 3.43 μm was 20-25% higher than that for generation of 3.31 μm. This can indeed be the case if the mid-IR losses are caused by the OH^- absorption peak centered near 2.86 μm. Up to 14 mW were generated at 3.3 μm with 0.92 W of pump and 0.25-0.3 W of signal in the waveguide. This amount of DFG radiation in the wavelength range 3-4 μm is 2 orders of magnitude higher than previously reported power levels generated by DFG in proton exchanged waveguides. The power level could not be sustained above 10 mW for more than a minute due to photorefractive effects.

Parametric amplification of 1560-nm radiation in reverse-proton exchanged waveguides (A. Sridharan with R. Roussev)

The advances in the understanding and design of waveguide devices for difference-frequency mixing of 1064-nm and 1560-nm radiation allowed the development of a waveguide device that solved problems that limited the maximum achievable pulse length and maximum gain of previous waveguide parametric amplifiers. The new design exploited a trade-off between confinement, losses at the mid-IR idler, and intensity of the parasitically generated green (second harmonic of the pump laser). The green was causing limitations of pulse length and maximum gain by green-induced infrared absorption. The new optimized design allowed increasing the maximum observed gain at 1560 nm from 21 to 45 dB, and the pulse length from 0.2 to 0.8 μs, which was the requirement for the intended application of narrow-line pulses for LIDAR-based wind-velocity measurements. The amplifier gain is plotted in fig. 23.
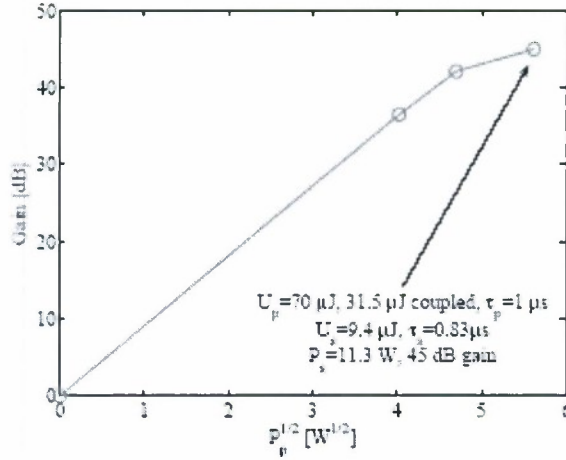
28

Figure 23: Gain of the waveguide OPA versus square root of peak pump power in the pulse

The observed gain saturation at high gain levels is due to pump depletion. At the maximum gain of 45 dB, the peak power in the output signal pulses was 11.3 W, and the energy in the pulse was 9.4 μJ. Green-induced infrared absorption was not a problem in this design at the power levels of operation. The parametric amplification was observed at 60 °C for 1 hour without signs of photorefractive degradation at the pump laser pulse repetition rate of 10 Hz. This project was partially supported by NASA.

Quasi-Group-Velocity Matching (QGVM) (J. Huang and X. Xie)

Using the waveguides that allow the use of a tight bend radius, we can fabricate OPG devices that use QGVM structures. The principle of periodic time-delays for compensating group-velocity dispersion (QGVM) was proven with a simple two-section device shown in fig. 24a. Between two sections of quasi-phase-matching gratings, two directional couplers are connected by one straight waveguide and one s-bend. The envelopes of the waves at 780 nm and 1560 nm will be matched at the end of the device if the length difference between the two paths is correctly designed. With the development of tighter low-loss waveguide bends, the same design can be used for near-degenerate OPG, as shown in fig. 24b.
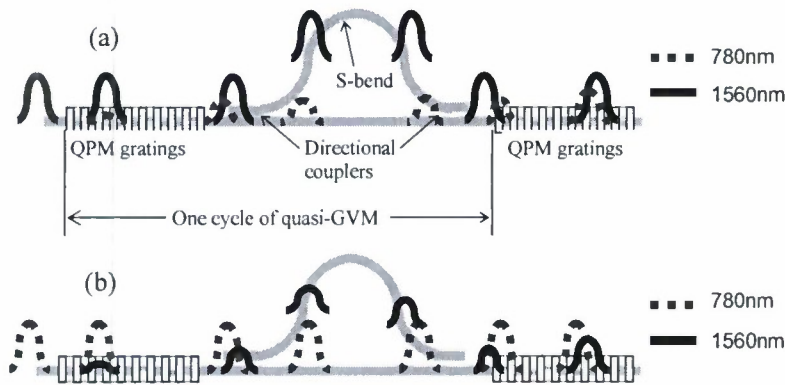

Figure 24: Diagram of waveguide devices with quasi-GVM. (a) for second harmonic generation, the 1560 nm wave is the pump; (b) for optical parametric generation, the 780 nm wave is the pump. The wavelength selective directional coupler and the delay sections put the faster wavelengths through a longer path length, periodically re-synchronizing the pulse envelopes, a discrete approximation to a group-velocity-matched structure (quasi-GVM).

29

SHG and OPG have different mechanisms. SHG generates coherent light while OPG is the amplification of noise. According to numerical simulations, we need four or more sections of quasi-phase-matching gratings on a device to observe the consequences of quasi-GVM in OPG. Unfortunately, with our typical reverse-proton-exchange recipe a 60-mm-long device can at most contain three sections of quasi-phase-matching gratings because the minimum bend radius with negligible propagation loss is 4 mm. We increase the proton-exchange depth from 1.84 μm to 2.39 μm to make tighter bends and overcome this problem. The annealing time is 23 hrs and the time of reverse-proton-exchange is 25 hrs. With this new recipe, the propagation loss in straight waveguides is <0.25 dB/cm for waves near 1560nm and <0.4 dB/cm for waves near 780nm. Although these are higher than the loss of <0.1 dB/cm with the old recipe, the minimum bend radius with negligible loss is now 1 mm instead of 4 mm. We are therefore able to design devices with five sections of QPM gratings on a 60-mm-long chip at the penalty of higher loss in the pump wave.

In the devices fabricated, each QPM grating is 5-mm long, which is about one walkoff length between the 2-ps-long pump pulses near 780 nm and the signal/idler pulses near 1560 nm. The devices begin from a single-mode filter for the pump, which is a segmented waveguide. The pump wave at 784 nm in the free-space TEM_{00} mode was converted into almost pure TM_{00} mode by the mode filter. Following the mode filter are five repeated copies of the structure shown in fig. 24b, ending with a section of QPM gratings. The waveguide width (defined as the opening on the SiO_2 mask) is 6.5 μm except in the mode filters. When the edge-to-edge spacing between the two arms of the directional couplers is 2 μm on mask, the coupling efficiency would be >95% for signal/idler waves near 1630 nm. The length of the S-bends was designed to almost completely compensate for the group velocity mismatch between the pump and signal/idler after each cycle. The chips were heated to 130°C to avoid significant photorefractive damage.
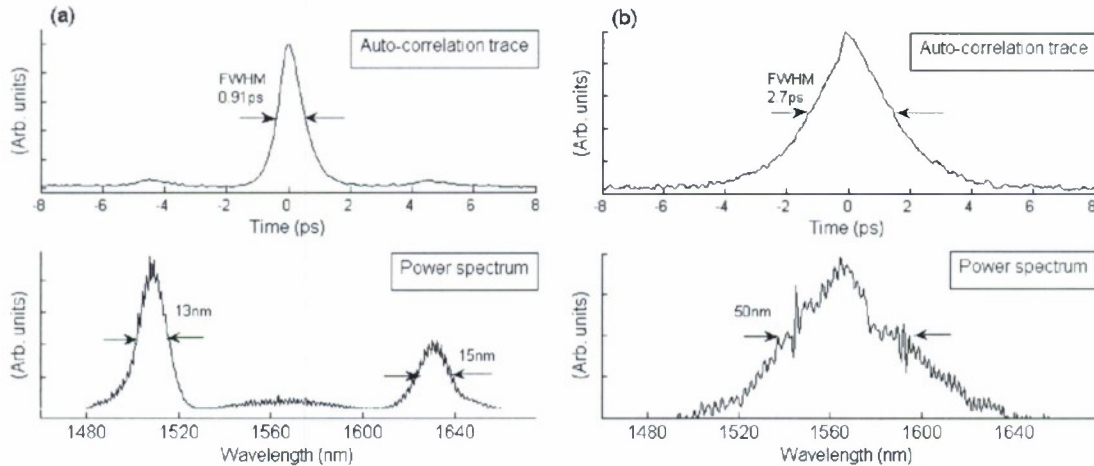

Figure 25:Auto-correlation traces and the power spectrum for the signal and idler from (a) quasi-GVM devices; (b) straight waveguides.

The OPG threshold in the devices with quasi-GVM was <100 pJ for signal and idler near 1560 nm, compared to a threshold of 200 pJ in a conventional device, which was one straight waveguide with a continuous 25-mm-long QPM grating.

Besides OPG threshold, we measured the pulse length of the signal and idler near 1.56 μm by autocorrelation using two-photon-absorption with a silicon detector and measured the power spectrum with an optical spectrum analyzer. Figure 25a shows the autocorrelation traces and the power spectrum for the signal and idler near 1560 nm when the depletion of the 784-nm pump was negligible. The bandwidth of the signal near 1510 nm was 13 nm, the bandwidth of the idler near 1630 nm was 15 nm, and the pulse length was 0.64 ps

(assuming a Gaussian pulse shape). The time-bandwidth-products of the signal and idler were both ~1.1. The spacing between the central peak and the tiny nearby peaks in the auto-correlation trace is exactly the temporal delay of a 5-mm-long waveguide. As a comparison, fig. 25b shows the auto-correlation traces and the power spectrum for the OPG output from a straight waveguide with a continuous 25-mm-long QPM grating. The bandwidth was >25 nm near degeneracy, the pulse length was ~1.9 ps, and the time-bandwidth-product was >5. The signal and idler waves from quasi-GVM devices are therefore much closer to the transform limit.

In summary, with quasi-group-velocity-matching in reverse-proton-exchange waveguides we demonstrated lower threshold and more coherent output from optical parametric generation. The OPG threshold was as low as 100 pJ and the time-band-width product of the signal and idler near 1560 nm was as low as 1.1.

The directional coupler limits the bandwidth of the quasi-GVM devices and is the bottleneck. More and more peaks appear when the signal/idler wavelengths are further away from degeneracy and the coupling efficiency of the directional coupler is decreasing. On the other hand, the amount of GVM compensation after each S-bend is relatively non-critical and we observed improvement in temporal properties both in over- and under-compensated conditions. We need more experiments to confirm this conclusion.

Highly-efficient waveguide SHG/SFG devices for frequency stabilization, nonlinear thresholding in OCDMA and single-photon detection (C. Langrock)

These devices, partially developed under support of DARPA Grant MDA972-03-1-0014 through Purdue Subgrant 531-03-6-01 on optical code-division multiple-access (OCDMA) device development, benefited from accurate modeling and optimization of the RPE waveguide designs partially supported by this program. It allowed devices with unprecedented efficiency to be implemented and used in experiments where low-power operation was critical. An RPE waveguide with a 4.6-cm long periodic poling and efficiency of ~2100 %/W (100%/Wcm²) allowed the generation of >10 mW output power at 760 nm with a 95 mW EDFA as the pump source. No AR coating was used in this demonstration. The device was used for demonstrating a simple and reliable scheme for frequency stabilization near 1.55 μm using frequency locking of the second harmonic to an iodine transition [Chui2005]. Further process optimization based on modeling and understanding of the proton diffusion process allowed further reduction of propagation losses without sacrificing conversion efficiency. Such highly efficient waveguides (3100 %/W in ~6 cm) were then used for low-power OCDMA system experiments [Jiang, 2005, 1 and 2] that demonstrated high system performance at practical optical power levels. In a related MURI program on photonic quantum information systems (DAAD19-03-1-0199), low-loss efficient waveguides based on these developments have been used for efficient detection of single photons in the 1.55- and 1.32-μm bands via SFG-based frequency conversion to the 700 nm band where highly efficient silicon-based single-photon detectors are available. [Langrock2005].

Frequency comb via RPE-PPLN waveguide (C. Langrock)

In collaboration with IMRA America, Inc., we developed a highly efficient low-loss RPE PPLN waveguide device to double the long wavelength part of a spectrally broadened mode-locked Er:fiber laser. The goal was it to build a low-noise highly efficient f-2f interferometer for carrier-envelope-phase locking needed for the generation of a stabilized frequency comb. This technique, pioneered by Prof. Theodor W. Haensch, allows the locking of the optical carrier frequency of a given laser oscillator to a highly stable RF oscillator. One implementation of this technique requires the laser's bandwidth to span at least an octave to allow for comparison between the high frequency part and the second harmonic of the low frequency part of the spectrum. This comparison is carried out by beat-note detection on a moderately fast photodiode. The error signal obtained this way can be used to lock the laser's carrier frequency to any reference oscillator. Doubling of the low frequency part of the spectrum used to be done in bulk nonlinear crystals. The optical power needed for the carrier envelope phase locking is obviously lost for metrology applications. Therefore, implementing a more efficient doubling method is of great importance. By using RPE PPLN waveguides we

were able to decrease the required pulse energy by 50% while increasing the resulting SNR by 10dB. Besides being more efficient, the waveguide geometry allowed for a fully integrated design by fiber pigtailing the oscillator directly to the PPLN chip. This resulted in a more stable and commercially viable implementation of carrier envelope phase locking. During the course of the measurements, we became aware of the fact that the generation of the octave spanning oscillator spectrum might also be carried out inside the very same PPLN waveguide, reducing the system complexity even further by eliminating the need for spectral broadening in a highly nonlinear fiber before spectral referencing. Experiments to investigate this option are currently being carried out.

II.2.5 Mid-IR Nonlinear Devices

Studies of Polarization-Dependence in an OP-GaAs Optical Parametric Oscillator (P.S. Kuo)

In related work on another QPM nonlinear optical material, the polarization dependence of three-frequency processes in orientation-pattererned GaAs was investigated. The high symmetry in the nonlinear susceptibility tensor of GaAs, together with isotropy in refractive index, leads to interesting polarization combinations of the three interacting waves. In fact, mixing of circularly polarized or depolarized light is allowed in OP-GaAs. In OP-GaAs samples, the beams propagate along the [-110] crystallographic direction, and the electric fields of the interacting waves all lie in the plane containing [001], [110], and [111]. We can calculate the gain associated with a polarization combination by considering the effective nonlinear coefficient, d_{eff}, which is calculated by considering the transverse projection of the nonlinear driving polarization. Figure 26 plots the expected magnitude of the effective nonlinear coefficient for different linear polarizations of the pump in an OP-GaAs OPO based on the assumption that the OPO will tend to oscillate with signal polarization that maximizes the parametric gain. Details of several key pump polarizations are shown in fig. 27. For the [110]-polarized case, we infer that if the signal wave is fixed to have [110] linear polarization, then an OP-GaAs OPO can be pumped with unpolarized light with $d_{eff} = d_{14}$.
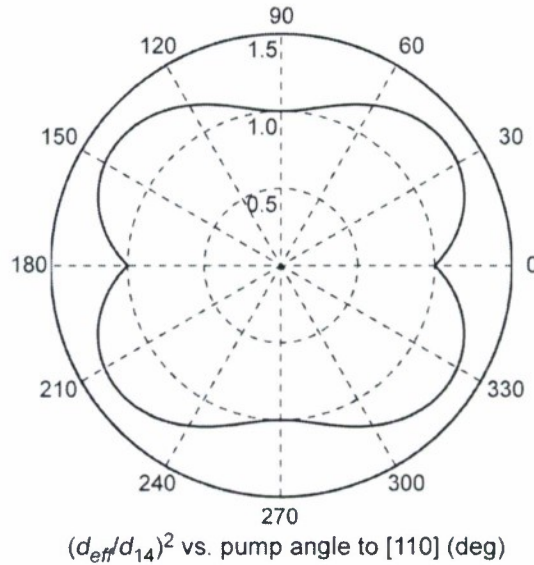

$(d_{eff}/d_{14})^2$ vs. pump angle to [110] (deg)

Figure 26: Relative gain, expressed as $(d_{eff}/d_{14})^2$, as a function of angle to the [110] crystallographic for a linearly polarized pump.

Pump Polarization	Signal Polarization	Idler Polarization	d_{eff}
[001]-linearly polarized	→	⇒	d_{14}
[111]-linearly polarized	↗	⇗	$\frac{2}{\sqrt{3}}d_{14}$
[110]-linearly polarized	Arbitrarily polarized signal	Idler complementary to signal	d_{14}
Circularly polarized	↻	↺	$\frac{1+\sqrt{5}}{2\sqrt{2}}d_{14}$

Figure 27: Expected OPO outputs and associated effective nonlinear coefficients for several pump polarizations.

An OP-GaAs optical parametric oscillator with nanosecond duration was constructed and used to probe effects of different pump polarizations. The OP-GaAs sample was 11-mm long, 6-mm wide, 600-μm thick and had 130-μm QPM period. The sample was pumped with 2.79-μm wavelength, 26-ns duration pulses with energy up to 65 μJ from a PPLN OPO that was in turn pumped with a Q-switched Nd:YAG laser. To change the orientation of the linear pump polarizations relative to the OP-GaAs crystal, the sample was rotated in the pump beam. The linearly polarized pulses from the PPLN OPO were converted to circular polarization using a quarter-wave plate formed with a MgF$_2$ Berek compensator (New Focus Model 5540). To produce pseudo-depolarized pump pulses, the output of the PPLN OPO was passed through a Lyot depolarizer.

Figure 28 plots the energy curves for [001]-, [110]-, [111]-linearly and circularly polarized pumps. From these curves, we estimated the threshold for the [111]-linearly polarized pump to be at 30 μJ while the thresholds for both the [001]- and [110]-linearly polarized pumps were at 41 μJ. The observations of identical thresholds for the [001]- and [110]-polarized cases and that the [111]-polarized pump threshold energy was 3/4 the size of the [001]-polarized case agree very well with theory, since the OPO threshold energy is proportional to $1/gain \propto 1/deff^2$. The threshold for the circularly polarized pump was about 29 μJ, which was slightly lower than the threshold for the [111]-linearly polarized pump. Theory predicts the circularly polarized pump to have slightly higher threshold than the [111]-linearly polarized case.

The OPO energy curve for the pseudo-depolarized pump is also plotted in figure 31. We observed the threshold for the depolarized pump at 50 μJ, which was only 22% higher than the threshold for the [001]-linearly polarized pump and only 67% larger than the [111]-polarized case. Also, at 55 μJ of pump energy (10% above threshold), we observed parametric oscillation for every pump pulse. Since the threshold for the depolarized pump is less than twice larger than that for the linearly polarized pump cases, we conclude that this is the first OPO to be pumped in a nontrivial way with a depolarized source. We note that the oscillation threshold with the depolarized pump was not as low as for the [001]-linearly polarized pump (as was hypothesized); further studies are needed to understand this difference.
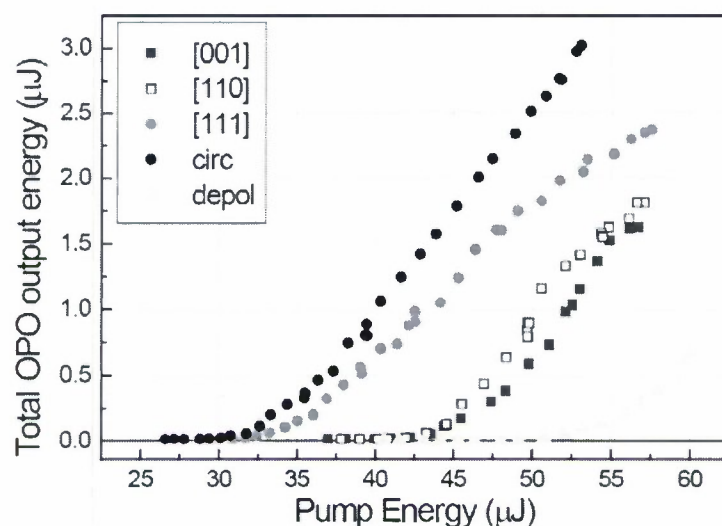
Figure 28: OP-GaAs OPO energy curves for [001]-, [110]-, and [111]-linearly polarized pumps, as well as circularly polarized and pseudo-depolarized pumps.

III. Directions for Continuing Research

The research described here has been highly productive in exploring new nonlinear materials, extending QPM technology, and developing new devices. Our long term research interests are in precisely these areas; exploring the limitations of vapor-transport-equilibrated materials, developing photorefraction-resistant waveguides, developing robust periodic poling for new wavelengths and new applications, and fabricating devices for high-power, visible generation, ultrafast applications, telecommunications applications and mid-IR generation applications. In light of our experience and successes in these areas, support for continued research along the same lines seems warranted.

IV. Program Participants

Martin M. Fejer	Principal Investigator
Robert L. Byer	Co-Investigator
Roger Route	Senior Research Associate
Konstantin Vodopyanov	Research Scientist
Carsten Langrock	Research Associate
Paulina Kuo	Post-Doctoral Associate
Ofer Levi	Post-Doctoral Associate
Mathieu Charbonneau-Lefort	Graduate Student Research Assistant, (Ph.D. awarded 2007)
Jie Huang	Graduate Student Research Assistant, (Ph.D. awarded 2007)
David Hum	Graduate Student Research Assistant, (Ph.D. awarded 2007)
Paulina Kuo	Graduate Student Research Assistant, (Ph.D. awarded 2007)
Carsten Langrock	Graduate Student Research Assistant, (Ph.D. awarded 2007)
Rostislav Roussev	Graduate Student Research Assistant, (Ph.D. awarded 2006)
Andrew Schober	Graduate Student Research Assistant, (Ph.D. awarded 2005)
Xiuping Xie	Graduate Student Research Assistant, (Ph.D. awarded 2006)

V. Publications Supported Directly

a) Mathieu Charbonneau-Lefort, Bedros Afeyan and M. M. Fejer,"Optical parametric amplifiers using chirped quasi-phase-matching gratings. II. Space-time evolution of light pulses", J. Opt. Soc. Am. B, Vol. 25, pp.683-700 (April 2008)

b) Mathieu Charbonneau-Lefort, Bedros Afeyan and M. M. Fejer,"Optical parametric amplifiers using chirped quasi-phase-matching gratings I: practical design formulas", J. Opt. Soc. Am. B, Vol. 25, pp.463 (March 2008)

c) P. S. Kuo, K. L. Vodopyanov, M. M. Fejer, X. Yu, J. S. Harris, D. F. Bliss, and D. Weyburne,, "GaAs optical parametric oscillator with circularly polarized and depolarized pump", Optics Letters, No. 18, Vol. 32, pp.2735-2737 (September 2007)

d) Carsten Langrock and M. M. Fejer,"Background-free collinear autocorrelation and frequency-resolved optical gating using mode multiplexing and demultiplexing in reverse-proton-exchange aperiodically poled lithium niobate waveguides", Optics Letters, No. 16, Vol. 32, pp.2306-2308 (August 2007)

e) Jie Huang, Carsten Langrock, X. P. Xie, and M. M. Fejer,"Monolithic 160 Gbit/s optical time-division multiplexer", Optics Letters, No. 16, Vol. 32, pp.2420-2422 (August 2007)

f) Carsten Langrock and Martin M. Fejer,"Fiber-feedback continuous-wave and synchronously-pumped singly-resonant ring optical parametric oscillators using reverse-proton-exchanged periodically-poled lithium niobate waveguides", Optics Letters, No. 15, Vol. 32, pp.2263-2265 (July 2007))

g) D. S. Hum, R. K. Route, G. D. Miller, V. Kondilenko, A. Alexandrovski, J. Huang, K. Urbanek, R. L. Byer, and M. M. Fejer,"Optical properties and ferroelectric engineering of vapor-transport-equilibrated, near-stoichiometric lithium tantalate for frequency conversion", Journal of Applied Physics, No. 9, Vol. 101, pp.093108 (May 2007)

h) D. S. Hum, R. K. Route and M. M. Fejer,"Quasi-phase-matched second-harmonic generation of 532 nm radiation in 25-degree-rotated, x-cut, near-stoichiometric, lithium tantalate fabricated by vapor transport equilibration", Optics Letters, No. 8, Vol. 32, pp.961-3 (April 2007)

i) Xiuping Xie and M. M. Fejer,"Cascaded optical parametric generation in reverse-proton-exchange lithium niobate waveguides", JOSA B, No. 3, Vol. 24, pp.585-591 (March 2007)

j) Carsten Langrock, Saurabh Kumar, John E. McGeehan, Alan Willner, M. M. Fejer,"All optical signal processing using χ2 nonlinearities in guided-wave devices", Journal of Lightwave Technology, No. 7, Vol. 24, pp.2579-2592 (July 2006)

k) Xiuping Xie, J. Huang, and M.M. Fejer,"Narrow-linewidth Near-Degenerate Optical Parametric Generation Achieved with Quasi-group-velocity-matching in Lithium Niobate waveguides", Optics Letters, No. 14, Vol. 31, pp.2190-2192 (July 2006)

l) Xiuping Xie, Jie Huang, and M.M. Fejer,"Narrow-linewidth near-degenerate optical parametric generation achieved with quasi-group-velocity-matching in lithium niobate waveguides", Optics Letters, No. 14, Vol. 31, pp.2190-2192 (July 2006)

m) Xiuping Xie, M. M. Fejer,"Two-spatial-mode parametric amplifier in lithium niobate waveguides with asymmetric Y junctions", Optics Letters, No. 6, Vol. 31, pp.799-801 (March 2006)

n) Jie Huang, X. P. Xie, Carsten Langrock, R. V. Roussev, D. S. Hum, and M. M. Fejer, "Amplitude modulation and apodization of quasi-phase-matched interactions", Optics Letters, No. 5, Vol. 31, pp.604-606 (March 2006)

o) Rostislav V. Roussev, Roger Route, Joseph Schaar, Karel Urbanek, Martin M. Fejer, Dieter Jundt, and Claudia Kajiyama,"Periodically poled vapor transport equilibrated lithium niobate for visible light generation", SPIE Proceedings, Nonlinear Frequency Generation and Conversion: Materials, Devices and Applications, Vol. 6103, pp.610302-1-7 (February 2006)

p) M. Schober, M. Charbonneau-Lefort, and M. M. Fejer,"Broadband quasi-phase-matched second-harmonic generation of ultrashort optical pulses with spectral angular dispersion", JOURNAL OF THE OPTICAL SOCIETY OF AMERICA B, No. 8, Vol. 22, pp.1699-1713 (August 2005)

q) M. Schober, M. M. Fejer, S. Carrasco, and L. Torner,"Engineering of multi-color spatial solitons with chirped-period quasi-phase-matching gratings in optical parametric amplification", OPTICS LETTERS, No. 15, Vol. 30, pp.1983-1985 (August 2005)

r) R. V. Roussev, R. Route, M. Katz, D. Jundt, C. Kajiyama, M. M. Fejer, "Vapor transport equilibrated lithium niobate resistant to photorefractive damage", Proc. SPIE Vol. 5710, p. 99-108 (2005)

s) M. Charbonneau-Lefort, B. Afeyan and M. M. Fejer. "Tandem chirped quasi-phase-matching grating optical parametric amplifier design for simultaneous group delay and gain control'', Optics Letters, 30, 634 (2005).

VI. Publications Supported through Facilities

Houxun Miao, Andrew M. Weiner, Carsten Langrock, Rostislav V. Roussev, and Martin M. Fejer,"Polarization-insensitive ultralow-power second-harmonic generation frequency-resolved optical gating", Optics Letters, No. 7 Vol. 32 pp.874-876 (April 2007)

Houxun Miao, Andrew M. Weiner, Carsten Langrock, Rostislav V. Roussev, and Martin M. Fejer,"Sensing and compensation of femtosecond waveform distortion induced by all-order polarization mode dispersion at selected polarization states", Optics Letters, No. 4 Vol. 32 pp.424-426 (February 2007)

W. C. Swann, J. J. McFerran, I. Coddington, N. R. Newbury, I. Hartl, M. E. Fermann, P. S. Westbrook, J. W. Nicholson, K. S. Feder, C. Langrock, and M. M. Fejer,"Fiber-laser frequency combs with sub-hertz relative linewidths", Optics Letters, No. 20 Vol. 31 pp.3046-3048 (October 2006)

Jian Wang, Junqiang Sun, J. R. Kurz, and M. M. Fejer,"Tunable Wavelength Conversion of ps-Pulses Exploiting Cascaded Sum- and Difference Frequency Generation in a PPLN-Fiber Ring Laser", IEEE Photonics Technology Letters, No. 20 Vol. 18, pp.2093-2095 (October 2006)

Paolo Minzioni, Ilaria Cristiani, Vittorio Degiorgio, Lucia Marazzi, Mario Martinelli, Carsten Langrock, M.M. Fejer,"Experimental demonstration of nonlinearity and dispersion compensation in an embedded link by optical phase conjugation", Photonics Technology Letters, No. 8 Vol. 18, pp.995-997 (May 2006)

Zh. Jiang, D. Seo; Sh. Yang, D.E. Leaird, R.V. Roussev, C. Langrock, M.M. Fejer, A.M.Weiner, "Four-user 10-Gb/s spectrally phase-coded O-CDMA system operating at ~30 fJ/bit", IEEE Phot. Techn. Lett. 17, no.3, p.705-7, (2005)

Z. Jiang, D. S. Seo, D.E. Leaird, R.V. Roussev, C. Langrock, M. M. Fejer, A. M. Weiner, "Reconfigurable all-optical code translation in spectrally phase-coded O-CDMA", Journ. Lightwave Techn. 23, no.6, p.1979-90, (2005)

C. Langrock, E. Diamanti, R.V. Roussev, Y.Yamamoto and M.M.Fejer, "Highly efficient single-photon detection at communication wavelengths by use of up-conversion in reverse-proton-exchanged periodically poled LiNbO$_3$ waveguide", Opt. Lett. 30, no.13, p.1725-7, (2005)

VII. References

[Hum]
D. S. Hum, R. K. Route and M. M. Fejer,"Quasi-phase-matched second-harmonic generation of 532 nm radiation in 25-degree-rotated, x-cut, near-stoichiometric, lithium tantalate fabricated by vapor transport equilibration", Optics Letters, No. 8, Vol. 32, pp.961-3 (April 2007)

[Roussev1]
R. V. Roussev, R. Route, M. Katz, D. Jundt, C. Kajiyama, M. M. Fejer, "Vapor transport equilibrated lithium niobate resistant to photorefractive damage", Proc. SPIE Vol. 5710, p. 99-108 (2005)

[Roussev2]
R. Roussev, A. Sridharan, K. Urbanek, R. Byer, M. Fejer, "Parametric amplification of 1.6 mu m signal in anneal- and reverse-proton exchanged waveguides", 2003 IEEE LEOS Annual Meeting Conference Proceedings, 27-28 Oct. 2003, Tucson, AZ, USA; p.334-5 vol.1

[Chui2005]
H-C. Chui, Y-W. Liu, J-T. Shy, S-Y. Shaw, R. V. Roussev, M. M. Fejer, "Frequency-stabilized 1520-nm diode laser with rubidium 5S{sub 1/2} to 7S{sub 1/2} two-photon absorption", Appl. Opt. 43, no.34, p.6348-51, (2004)

[Jiang2005-1]
Zh. Jiang, D. Seo; Sh. Yang, D.E. Leaird, R.V. Roussev, C. Langrock, M.M. Fejer, A.M.Weiner, "Four-user 10-Gb/s spectrally phase-coded O-CDMA system operating at ~30 fJ/bit", IEEE Phot. Techn. Lett. 17, no.3, p.705-7, (2005)

[Jiang2005-2]
Z. Jiang, D. S. Seo, D.E. Leaird, R.V. Roussev, C. Langrock, M. M. Fejer, A. M. Weiner, "Reconfigurable all-optical code translation in spectrally phase-coded O-CDMA", Journ. Lightwave Techn. 23, no.6, p.1979-90, (2005)

[Langrock2005]
C. Langrock, E. Diamanti, R.V. Roussev, Y.Yamamoto, M.M.Fejer, "Highly efficient single-photon detection at communication wavelengths by use of upconversion in reverse-proton-exchanged periodically poled $LiNbO_3$ waveguide", Opt. Lett. 30, no.13, p.1725-7, (2005)